Electronic Supplementary Material (ESI) for New Journal of Chemistry.

Monosubstituted pillar[5]arene functionalized with (amino)phosphonate fragments are “smart” building blocks for constructing nanosized structures with some s- and p-metal cations in the organic phase

Anastasia A. Nazarova,[a] Luidmila S. Yakimova,[a] Pavel L. Padnya,[a] Yladimir G. Evtugyn,[b] Yuri N. Osin,[b] Peter J. Cragg,[c] Ivan I. Stoikov[a]*

[a]A.M.Butlerov Chemical Institute, Kazan Federal University, 420008 Kremlevskaya, 18, Kazan, Russian Federation. Fax:+7 843 275 2253; Tel: +7 843 233 7462; E-mail: Ivan.Stoikov@mail.ru

[b]Interdisciplinary Center for Analytical Microscopy, Kazan Federal University, 420008 Kremlevskaya, 18, Kazan, Russian Federation.

[c]School of Pharmacy and Biomolecular Sciences, University of Brighton, Huxley Building, Moulsecoomb. Brighton, East Sussex BN2 4GJ, UK;

*Corresponding author. Tel.: +7-843-2337462; fax: +7-843-2752253; e-mail: Ivan.Stoikov@mail.ru

Electronic Supplementary Information (44 pages)

Fig. S1. ^{1}H NMR spectrum of 4-hydroxy-8,14,18,23,26,28,31,32,35-nonamethoxypillar[5]arene *(2)*, $CDCl_3$, 298 K, 400 MHz.

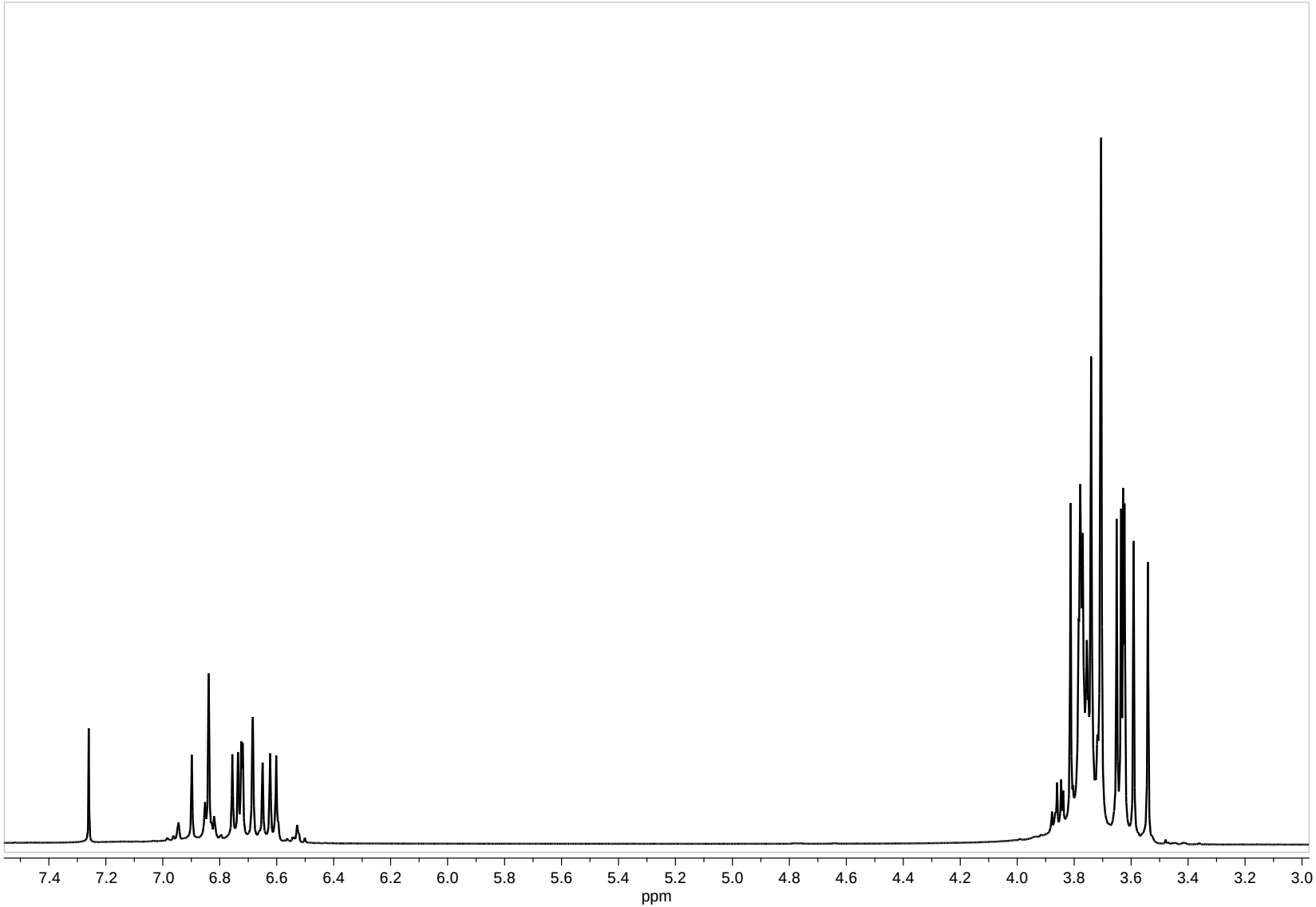

Fig. S2. ^{1}H NMR spectrum of 4-[(O,O-diethyl)-phosphoryl-1-oxymethylene]-8,14,18,23,26,28,31,32,35-nonamethoxypillar[5]arene (*3*), $CDCl_3$, 298 K, 400 MHz.

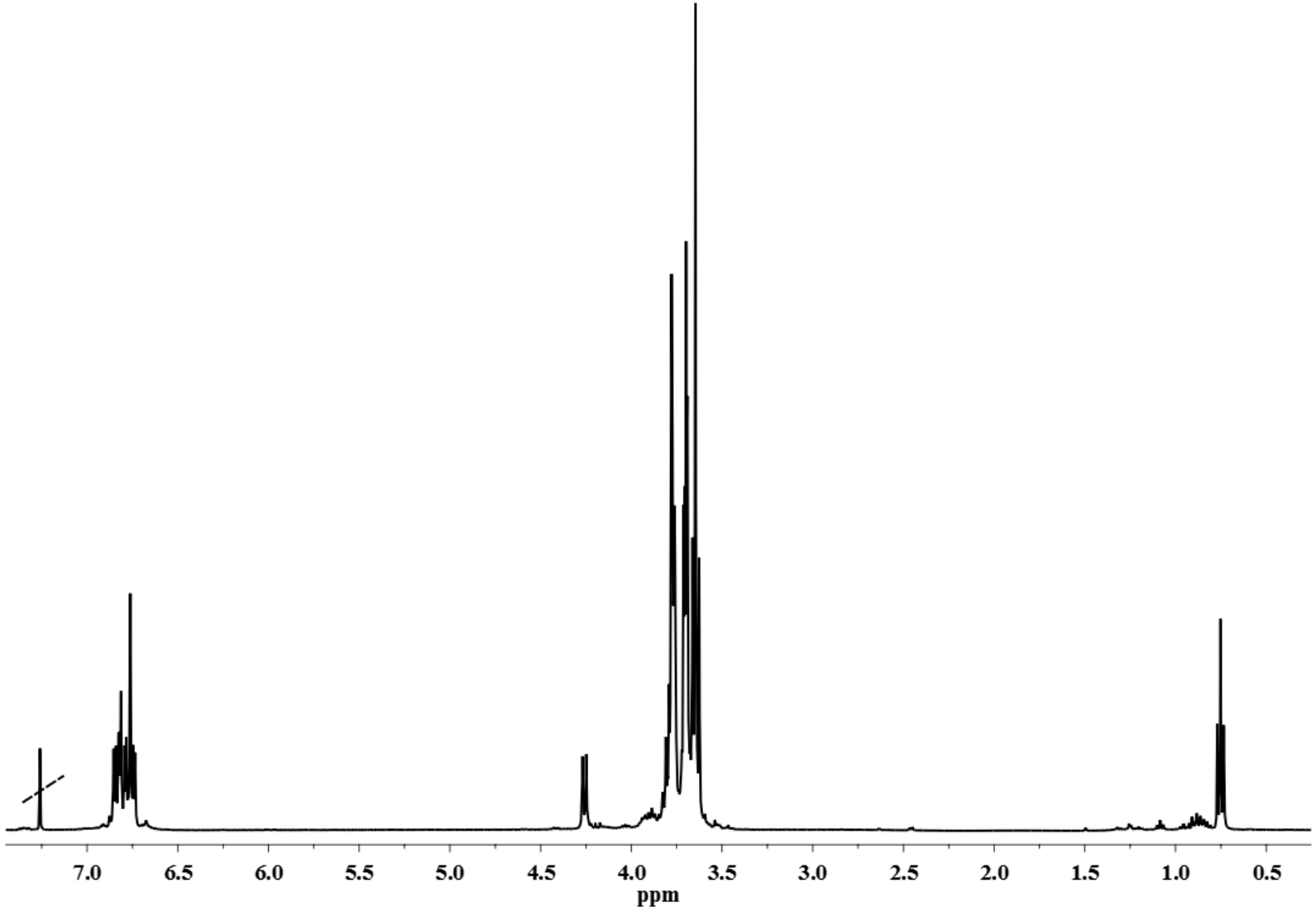

Fig. S3. ^{1}H NMR spectrum of 4,8,14,18,23,26,28,31,32-nonamethoxy-35-{N-[1-(O,O-diethylphosphoryl)-1-methylethyl]-(3'-aminopropoxy}-pillar[5]arene *(4)*, $CDCl_3$, 298 K, 400 MHz.

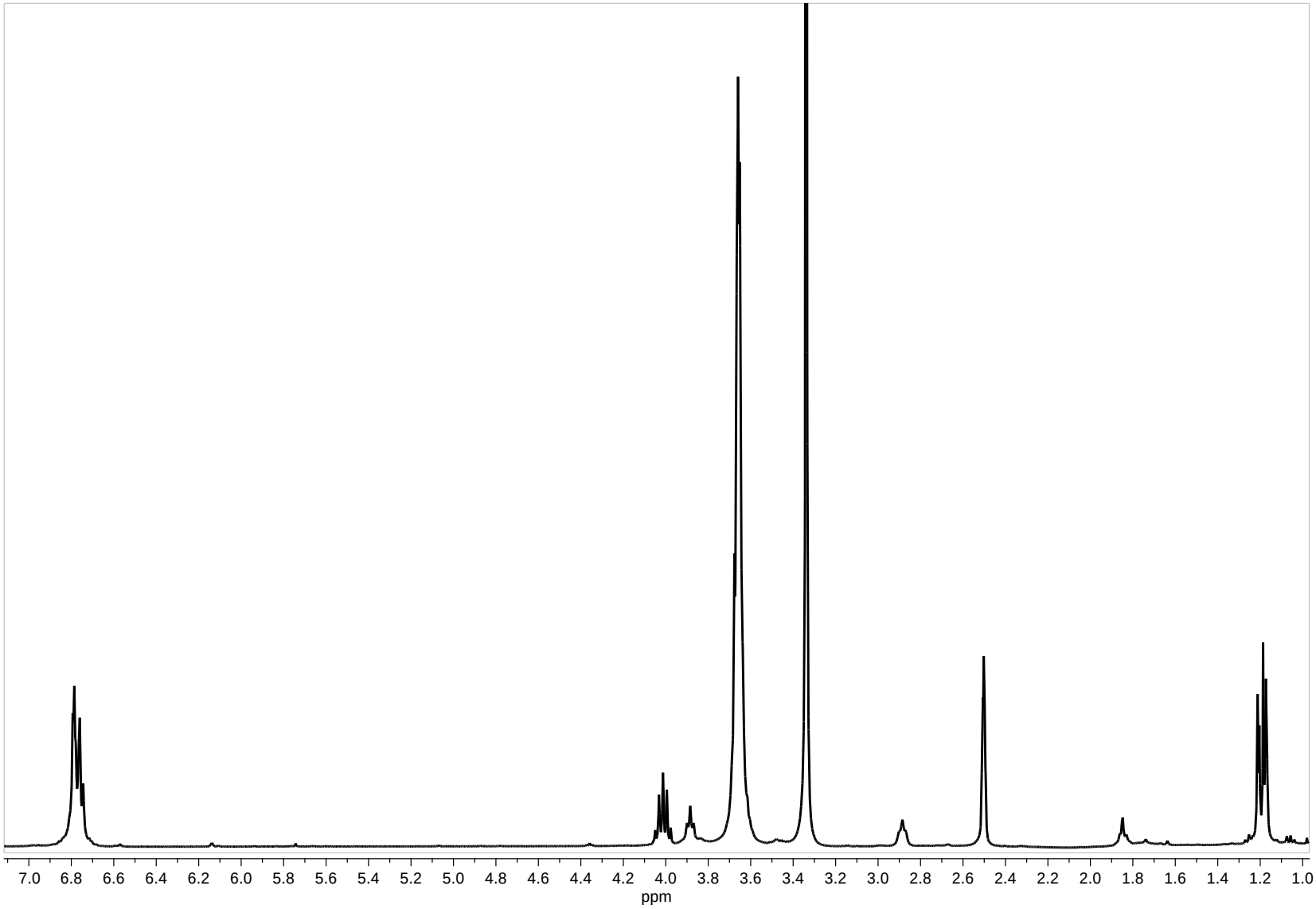

Fig. S4. ^{1}H NMR spectrum of 4,8,14,18,23,26,28,31,32-nonamethoxy-35-{N-[1-(O,O-diethylphosphoryl)-1-cyclopentyl]-(3'-aminopropoxy}-pillar[5]arene *(5)*, $CDCl_3$, 298 K, 400 MHz.

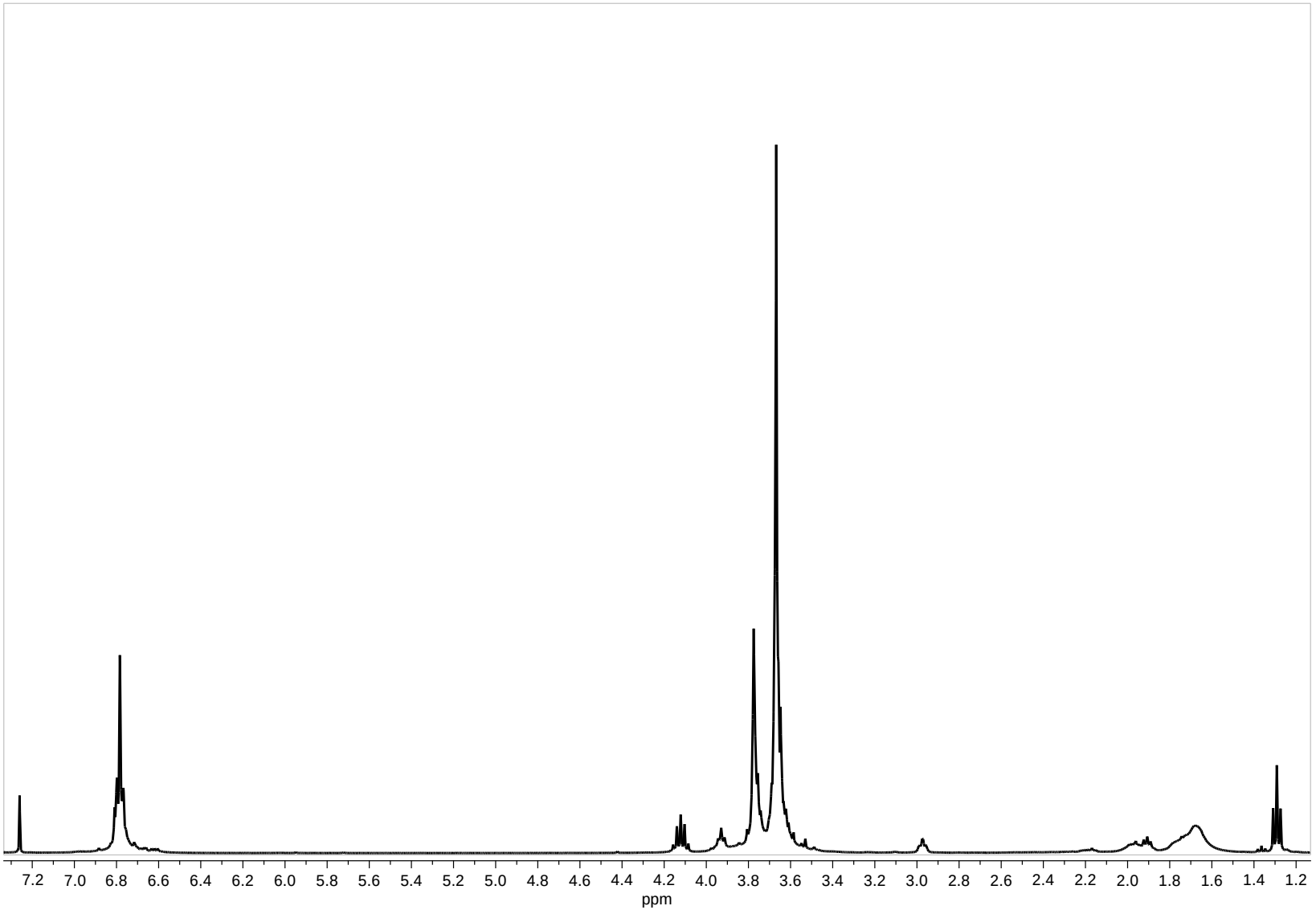

Fig. S5. ^{1}H NMR spectrum 4,8,14,18,23,26,28,31,32-nonamethoxy-35-{N-[1-(O,O-diethylphosphoryl)-1-cyclohexyl]-(3'-aminopropoxy}-pillar[5]arene *(6)*, $CDCl_3$, 298 K, 400 MHz.

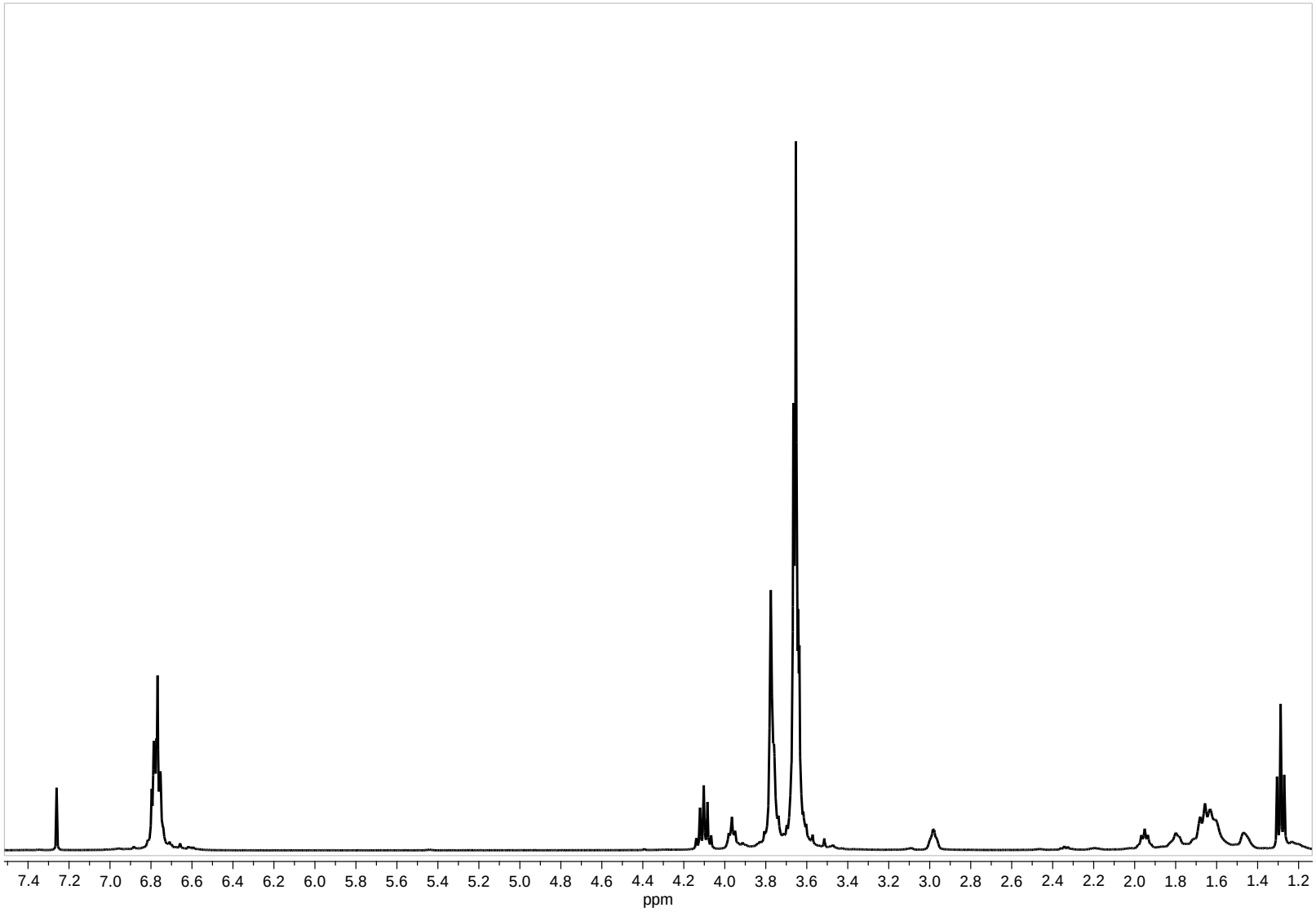

Fig. S6. ^{31}P NMR spectrum of 4-[(O,O-diethyl)-phosphoryl-1-oxymethylene]-8,14,18,23,26,28,31,32,35-nonamethoxypillar[5]arene (*3*), CDCl3, 298 K, 162 MHz.

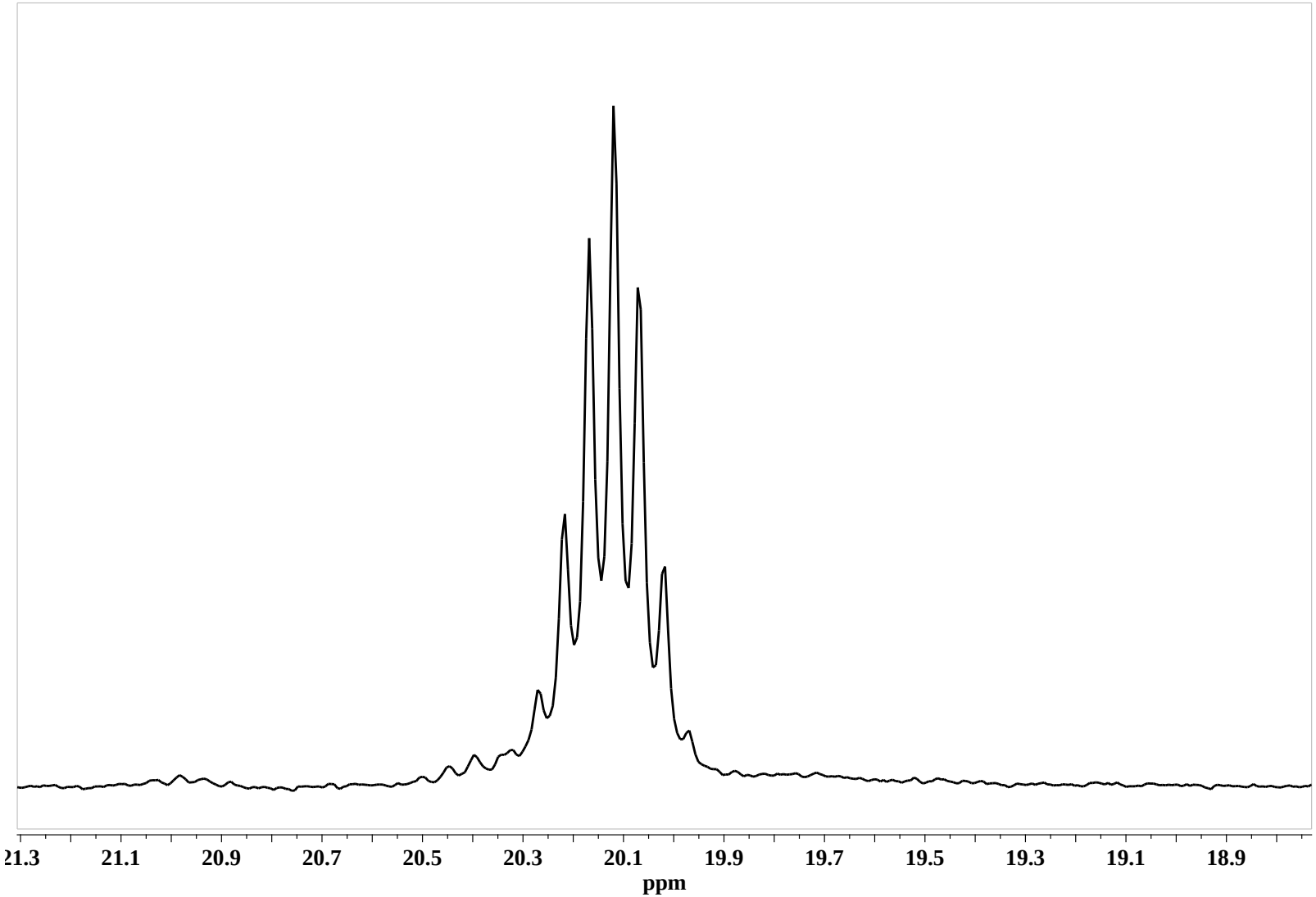

Fig. S7. $^{31}P\{^{1}H\}$ NMR spectrum of 4,8,14,18,23,26,28,31,32-nonamethoxy-35-{N-[1-(O,O-diethylphosphoryl)-1-methylethyl]-(3'-aminopropoxy}-pillar[5]arene *(4)*, $CDCl_3$, 298 K, 162 MHz.

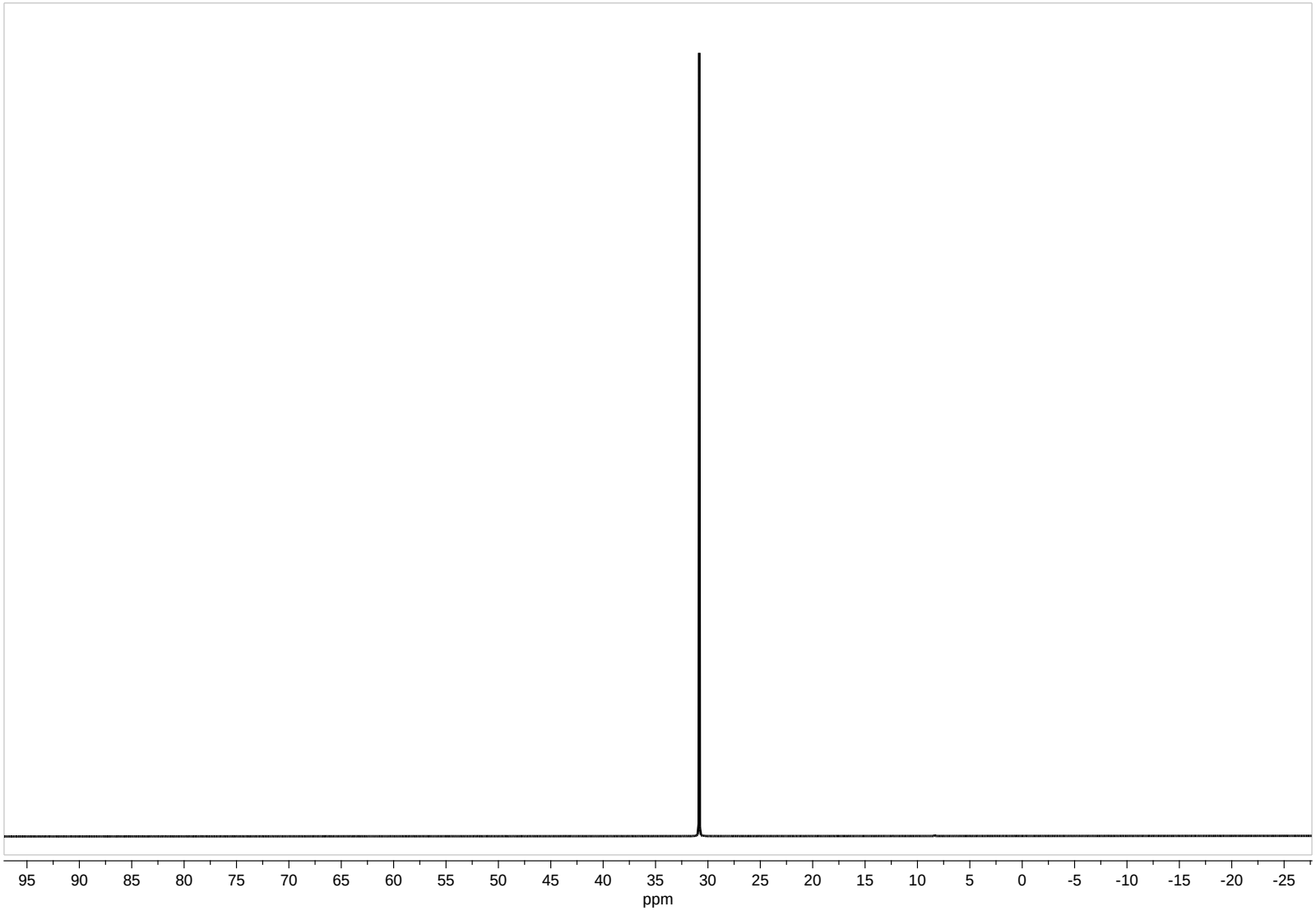

Fig. S7. $^{31}P\{^{1}H\}$ NMR spectrum of 4,8,14,18,23,26,28,31,32-nonamethoxy-35-{N-[1-(O,O-diethylphosphoryl)-1-cyclopentyl]-(3'-aminopropoxy}-pillar[5]arene *(5)*, $CDCl_3$, 298 K, 162 MHz.

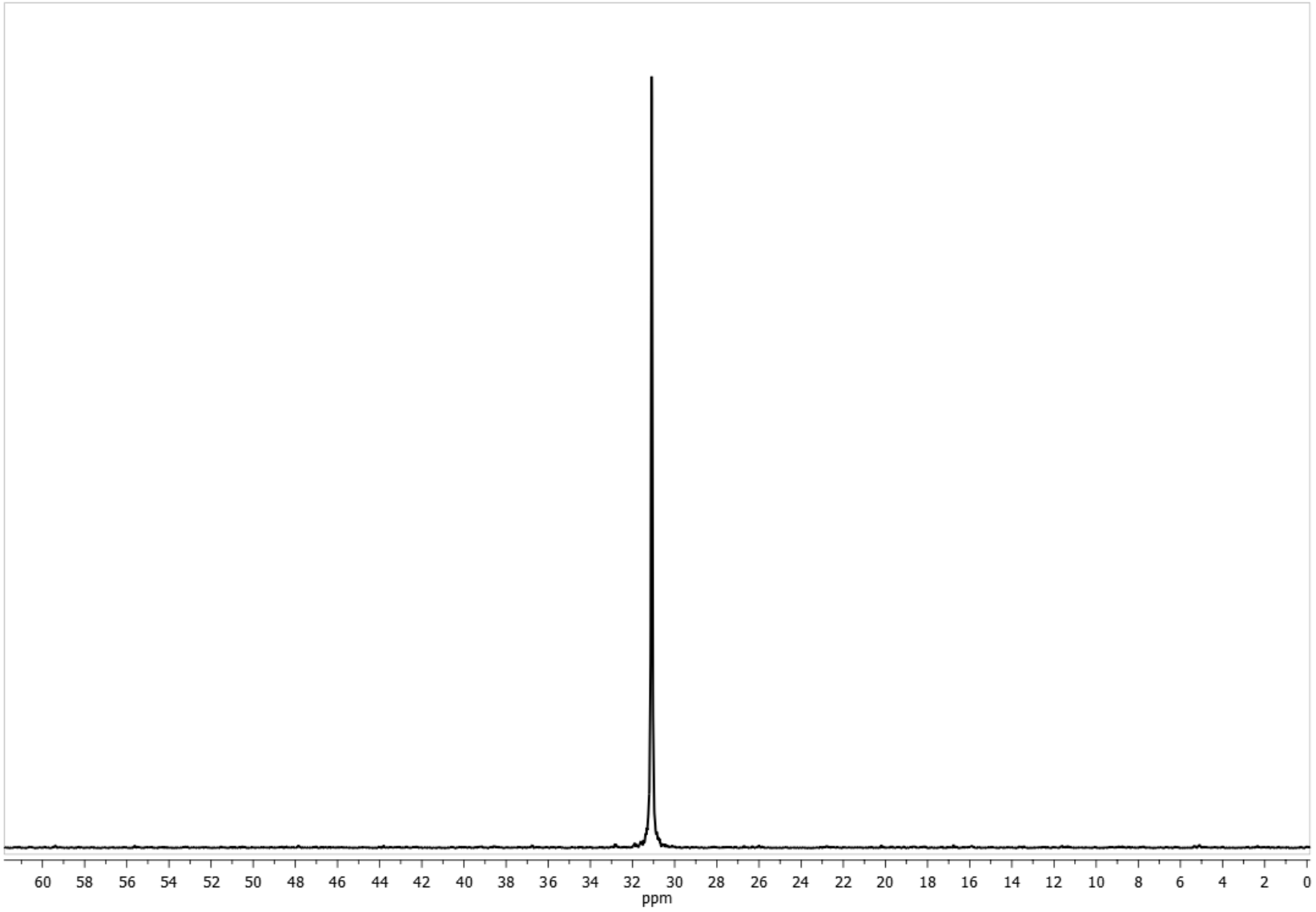

Fig. S8. $^{31}P\{^{1}H\}$ NMR spectrum 4,8,14,18,23,26,28,31,32-nonamethoxy-35-{N-[1-(O,O-diethylphosphoryl)-1-cyclohexyl]-(3'-aminopropoxy}-pillar[5]arene *(6)*, $CDCl_3$, 298 K, 162 MHz.

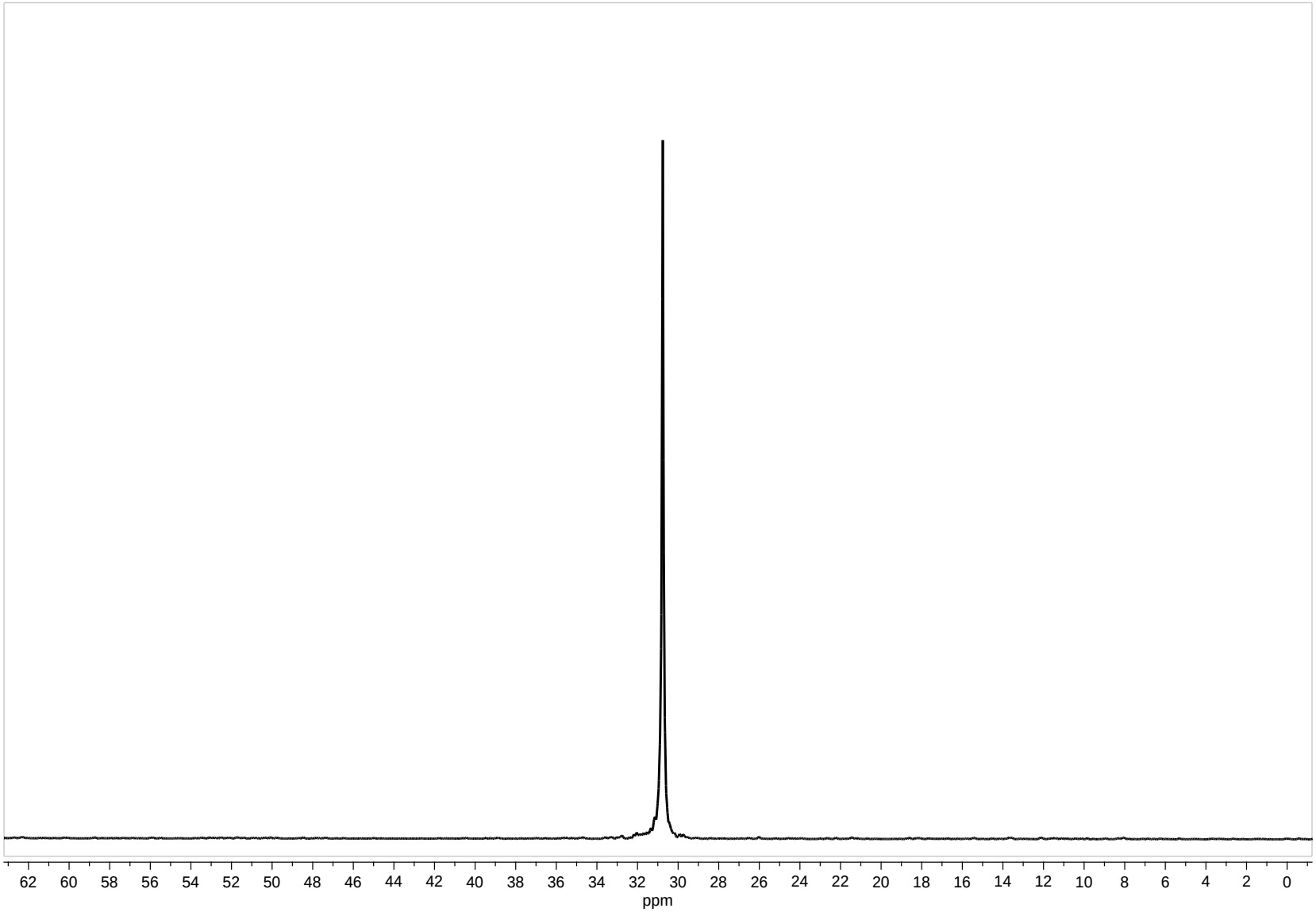

Fig. S9. ^{13}C NMR spectrum of 4-[(O,O-diethyl)-phosphoryl-1-oxymethylene]-8,14,18,23,26,28,31,32,35-nonamethoxypillar[5]arene (3), CDC_3, 298 K, 100 MHz.

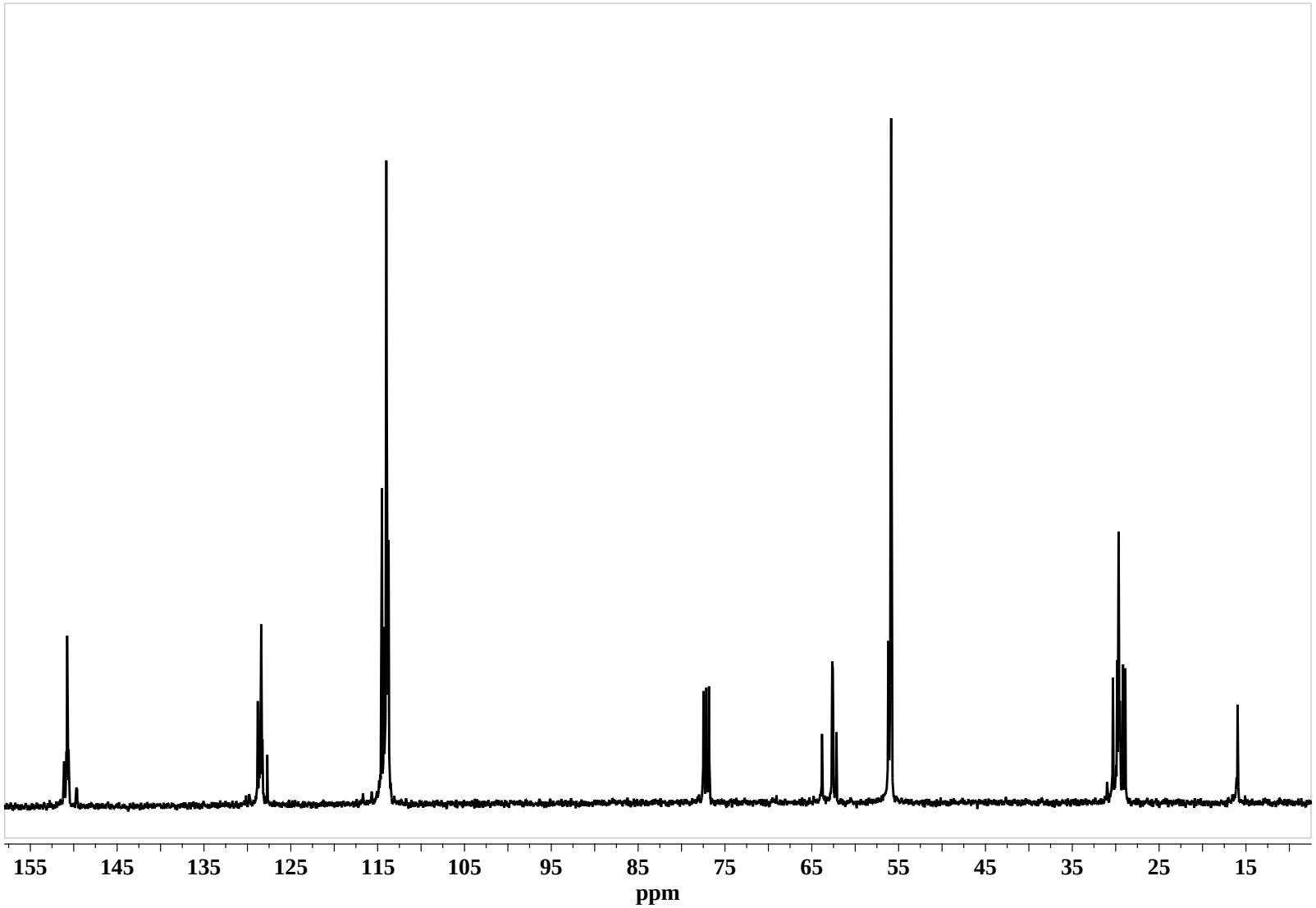

Fig. S10. Mass spectrum (ESI) of 4-[(O,O-diethyl)-phosphoryl-1-oxymethylene]-8,14,18,23,26,28,31,32,35-nonamethoxypillar[5]arene (3).

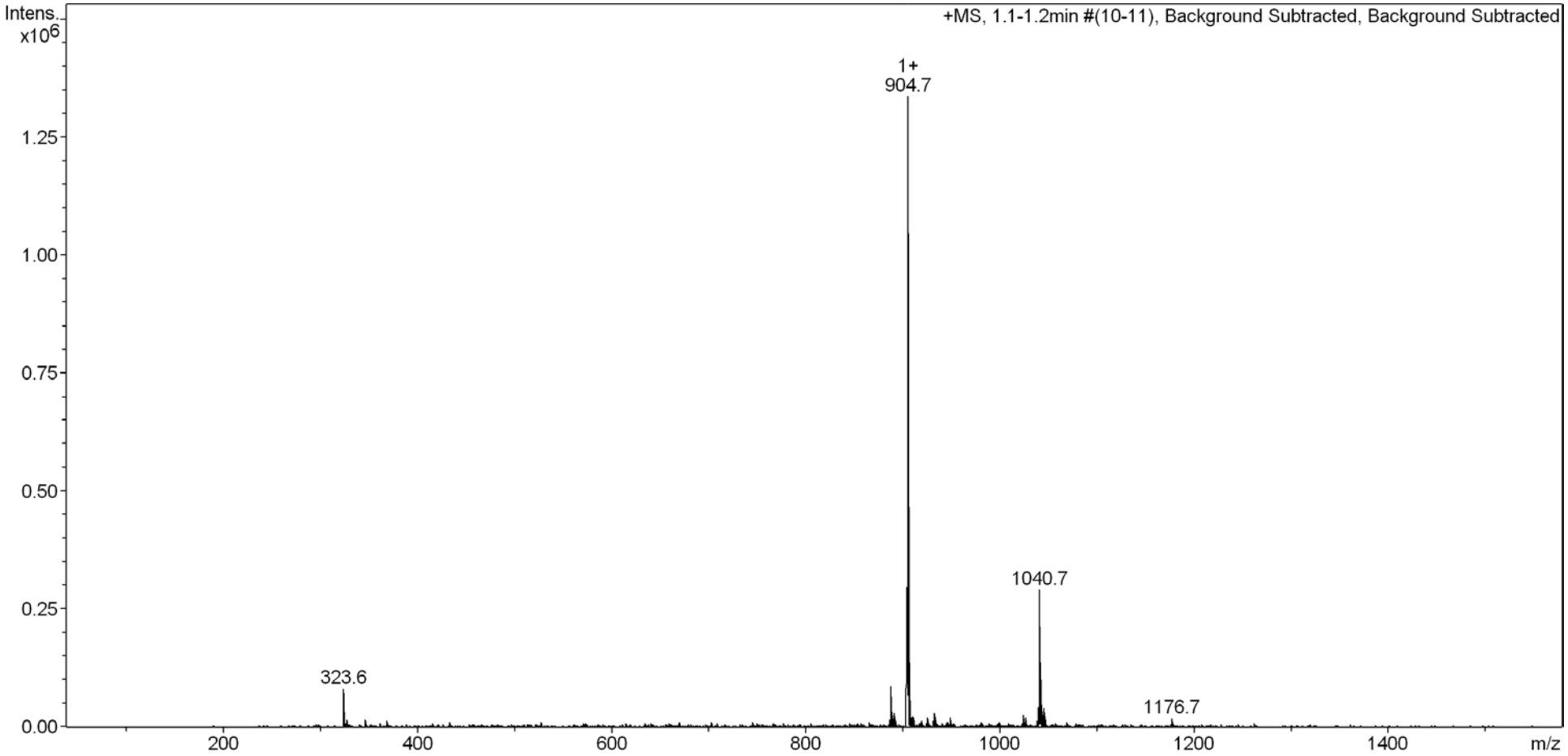

Fig. S11. IR spectrum of 4-[(O,O-diethyl)-phosphoryl-1-oxymethylene]-8,14,18,23,26,28,31,32,35-nonamethoxypillar[5]arene (3).

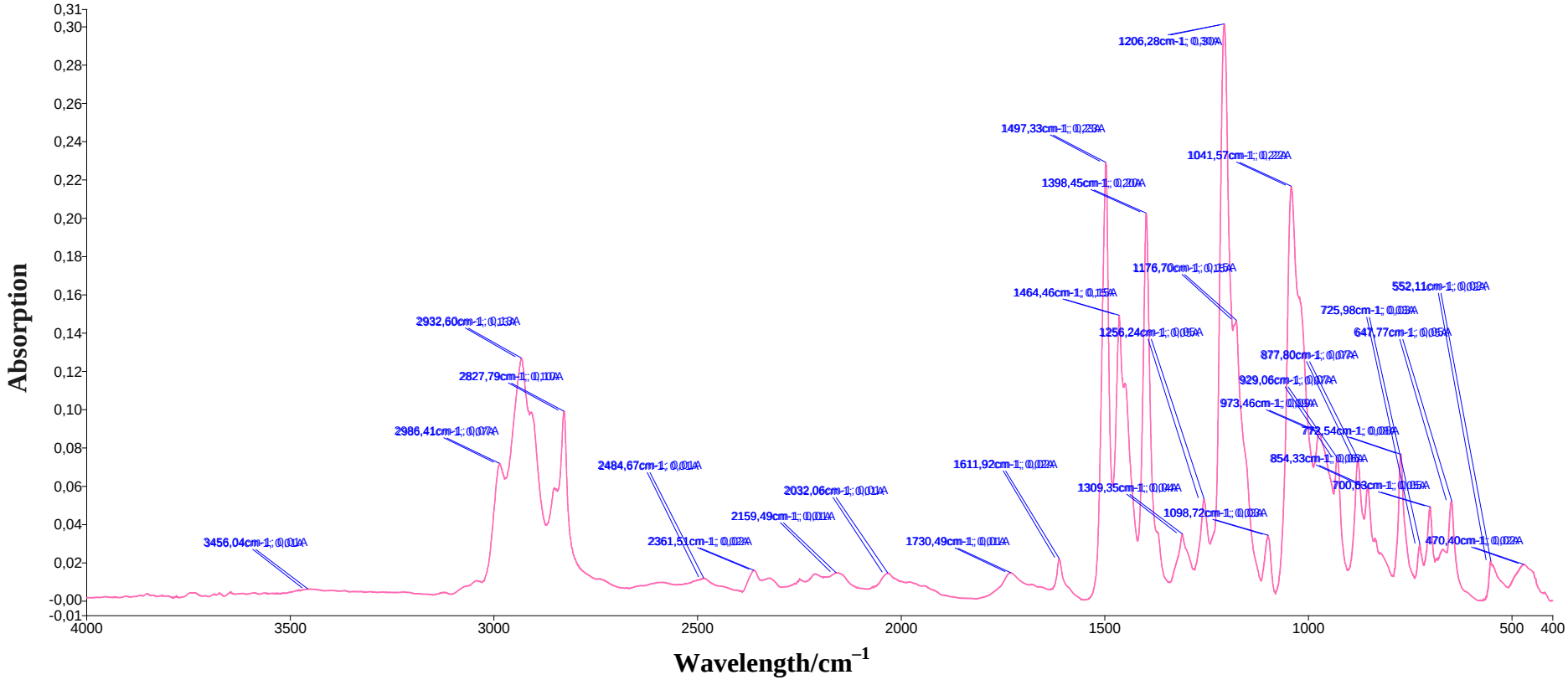

Determination of the stability constant and stoichiometry of the complex by the UV titration

The UV measurements were performed with "Shimadzu UV-3600" instrument. The $1 \cdot 10^{-2}$ M solution of the guest (15, 30, 45, 60, 75, 90, 105, 120, 135 and 150 µl) in MeOH was added to 0.3 ml of the solution of **3**-**6** ($5 \cdot 10^{-4}$ M) in $CHCl_3$ and diluted to final volume of 3 ml with $CHCl_3$. The UV spectra of the solutions were then recorded. The stability constant and stoichiometry of complexes were calculated as described below. Three independent experiments were carried out for each series. Student's *t*-test was applied in statistical data processing.

The system equilibrium is described by Eq. (1), where H, G, G_nH denote the macrocycles **3**-**6**, guests (Na^+, Cs^+, K^+, Pb^{2+}), complex with guests, n – number of the guest with one macrocycle.

$$nG + H \Leftrightarrow G_nH \qquad (1)$$

The association constant, K_{ass}, is defined by Eq. (2).

$$K_{ass} = [G_nH] / [G]^n [H] \qquad (2)$$

To determine the stoichiometry coefficient n of the complexes forming in the water Eq. (2) was converted into Eq. (3).

$$\lg K_{ass} = \lg [G_nH] - n \lg [G] - \lg [H] \qquad (3)$$

The solution absorbance A, is a sum of those related to complex, host and guest (A_{GnH}, A_H and A_G, respectevly) is equal to:

$$A = A_{GnH} + A_H + A_G \qquad (4)$$

Assuming that the Beer-lambert law is obeyed for all the components considered Eq. 5, the absorbance A is expressed as:

$$A_i = c_i \varepsilon_i l \qquad (5)$$

where c_i is a molar concentration of i-species, ε_i is the molar absorptivity, and *l* is the cell thickness. For complexation between the host and guest the absorbance mesurement is commonly conducted at the wavelength of absorbance maximum in the charge-transfer region where $A_G=0$. This gives Eq. 6.

$$A = A_{GnH} + A_H \qquad (6)$$

Concentration of the complex [G_nH] in the system is calculated according to equations (5) and (6).

The plot of lg [G_nH]- lg [H] versus lg [G] (Fig. S12) presents a straight line, slope of which equals to n. Assotiation constants K_{ass} are calculated using the intercept values (b).

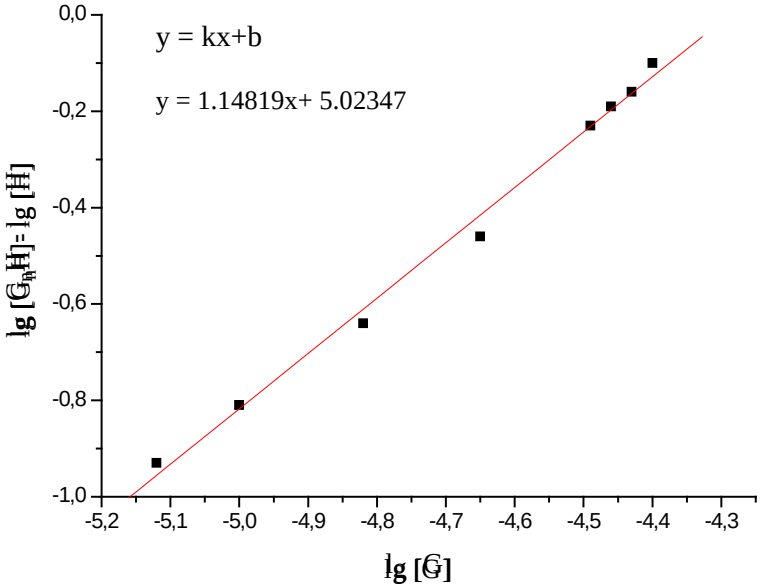

Fig. S12. Plot of lg [G_nH]- lg [H] versus lg [G] host/guest system.

$$b = \lg K_{acc} \qquad (7)$$

Fig. S13. The spectrophotometric titration of the system pillar[5]arene 3 and $CsNO_3$ in $CHCl_3$ + 5% CH_3OH.

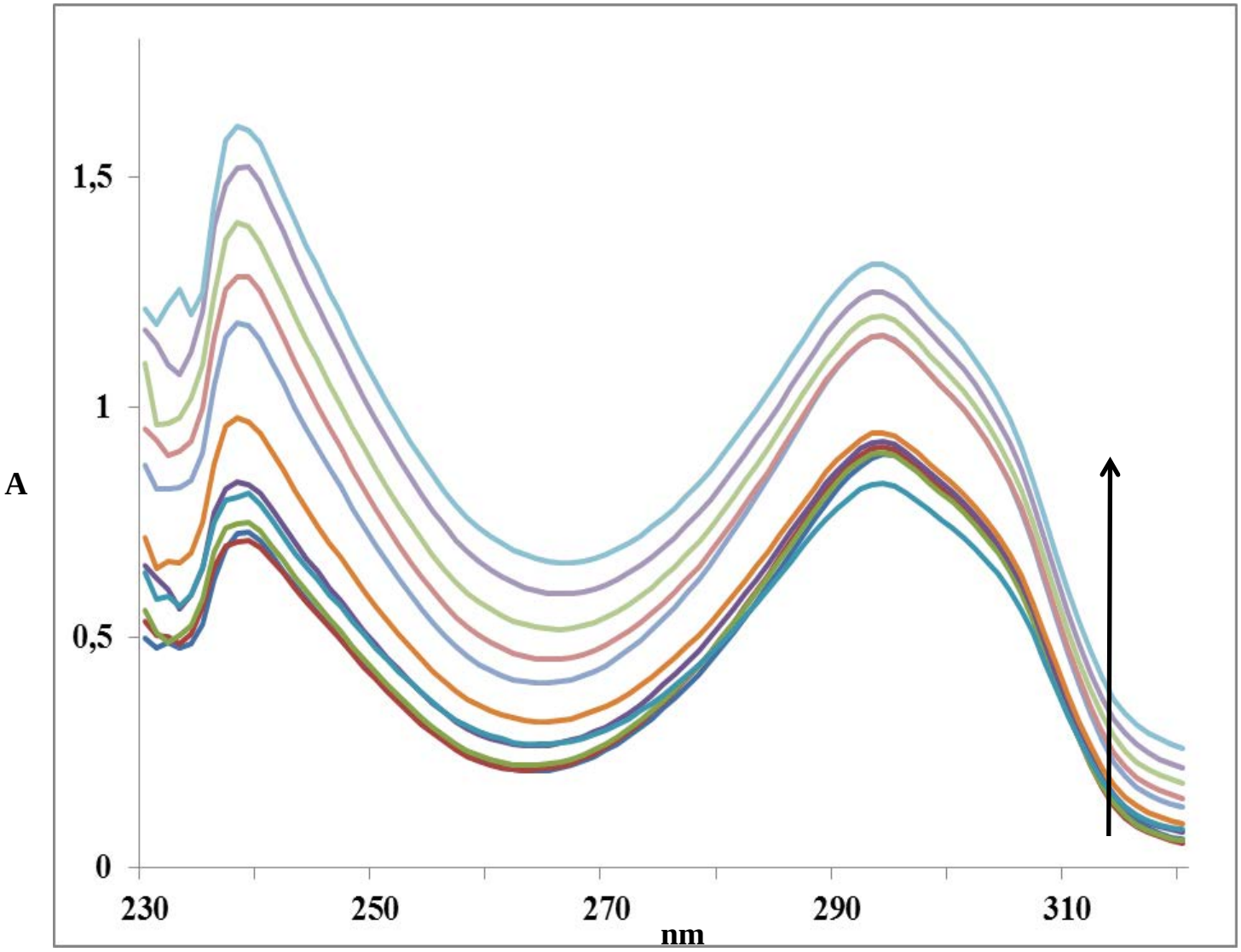

Fig. S14. The spectrophotometric titration of the system pillar[5]arene 3 and $Pb(NO_3)_2$ in $CHCl_3$ + 5% CH_3OH.

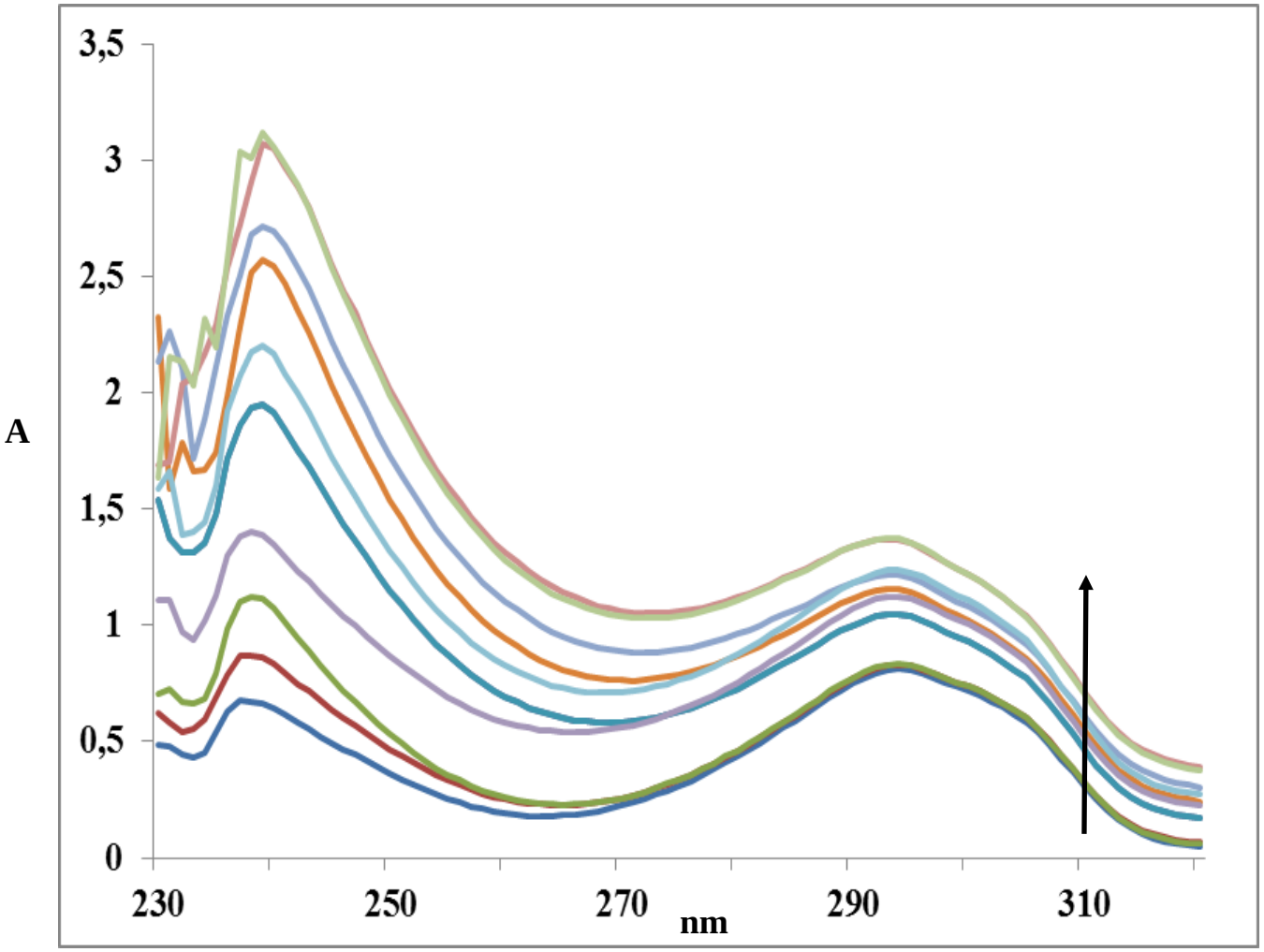

Fig. S15. The spectrophotometric titration of the system pillar[5]arene 4 and $NaNO_3$ in $CHCl_3$ + 5% CH_3OH.

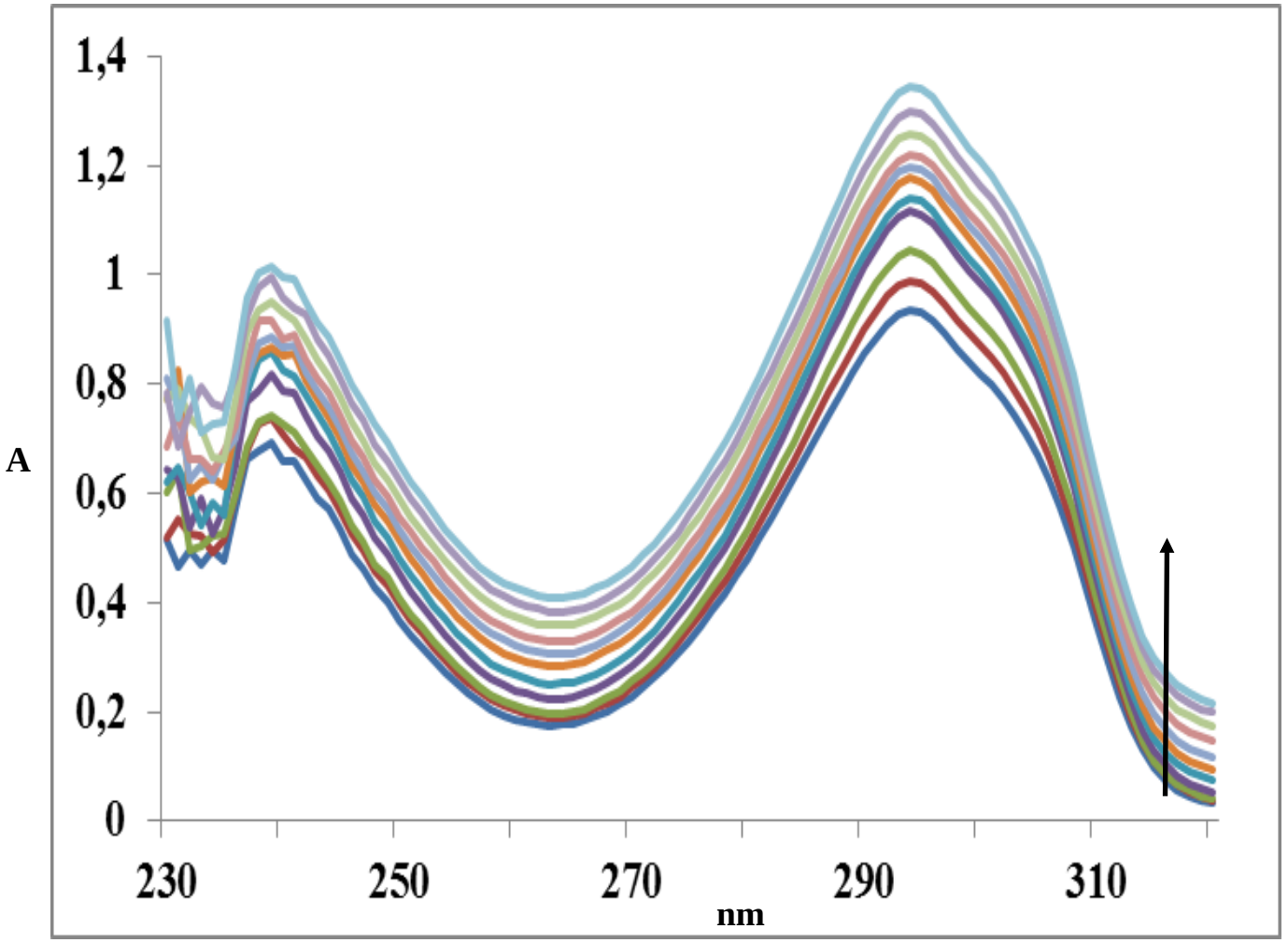

Fig. S16. The spectrophotometric titration of the system pillar[5]arene 4 and $CsNO_3$ in $CHCl_3$ + 5% CH_3OH.

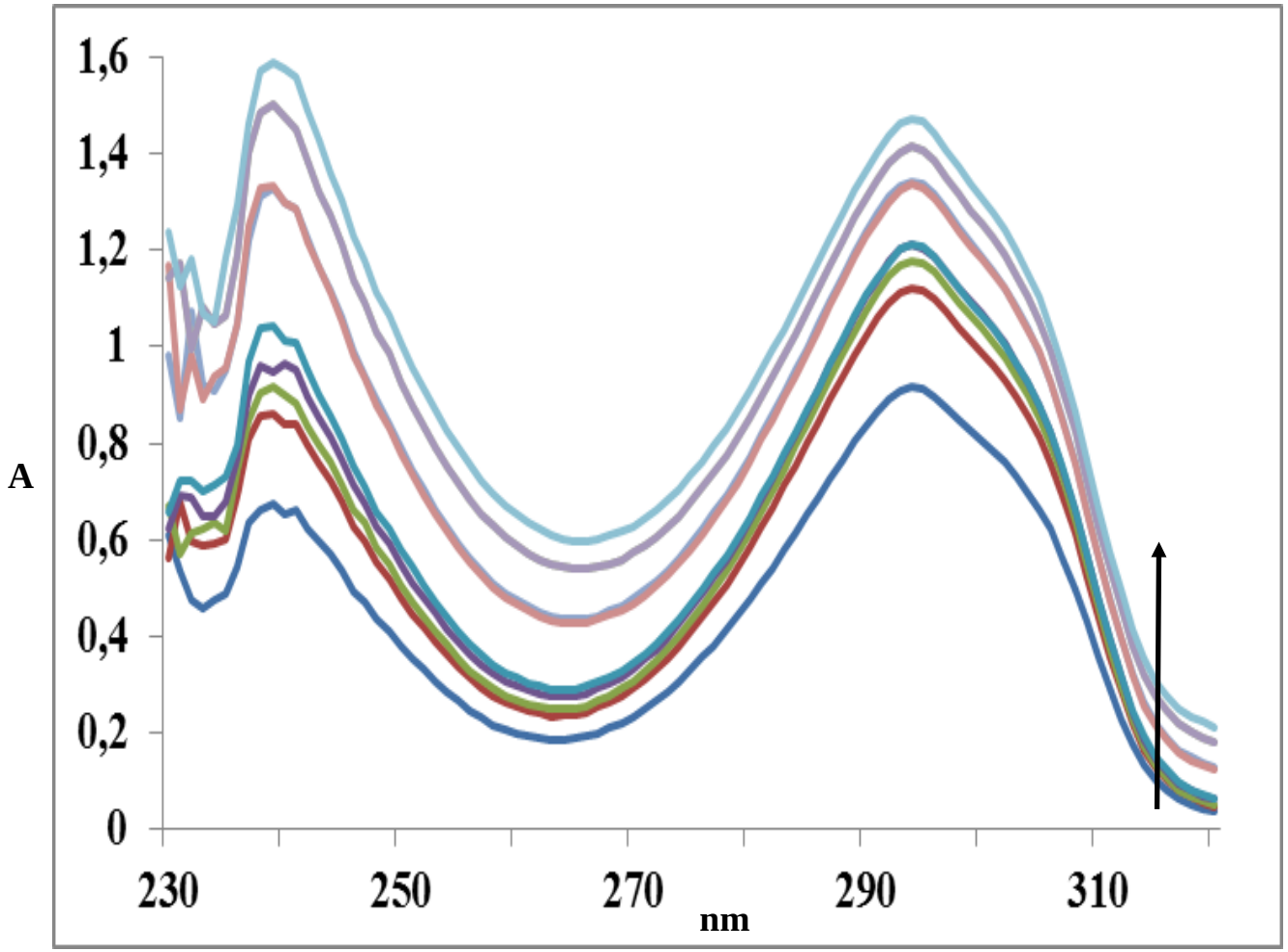

Fig. S17. The spectrophotometric titration of the system pillar[5]arene 4 and $Pb(NO_3)_2$ in $CHCl_3$ + 5% CH_3OH.

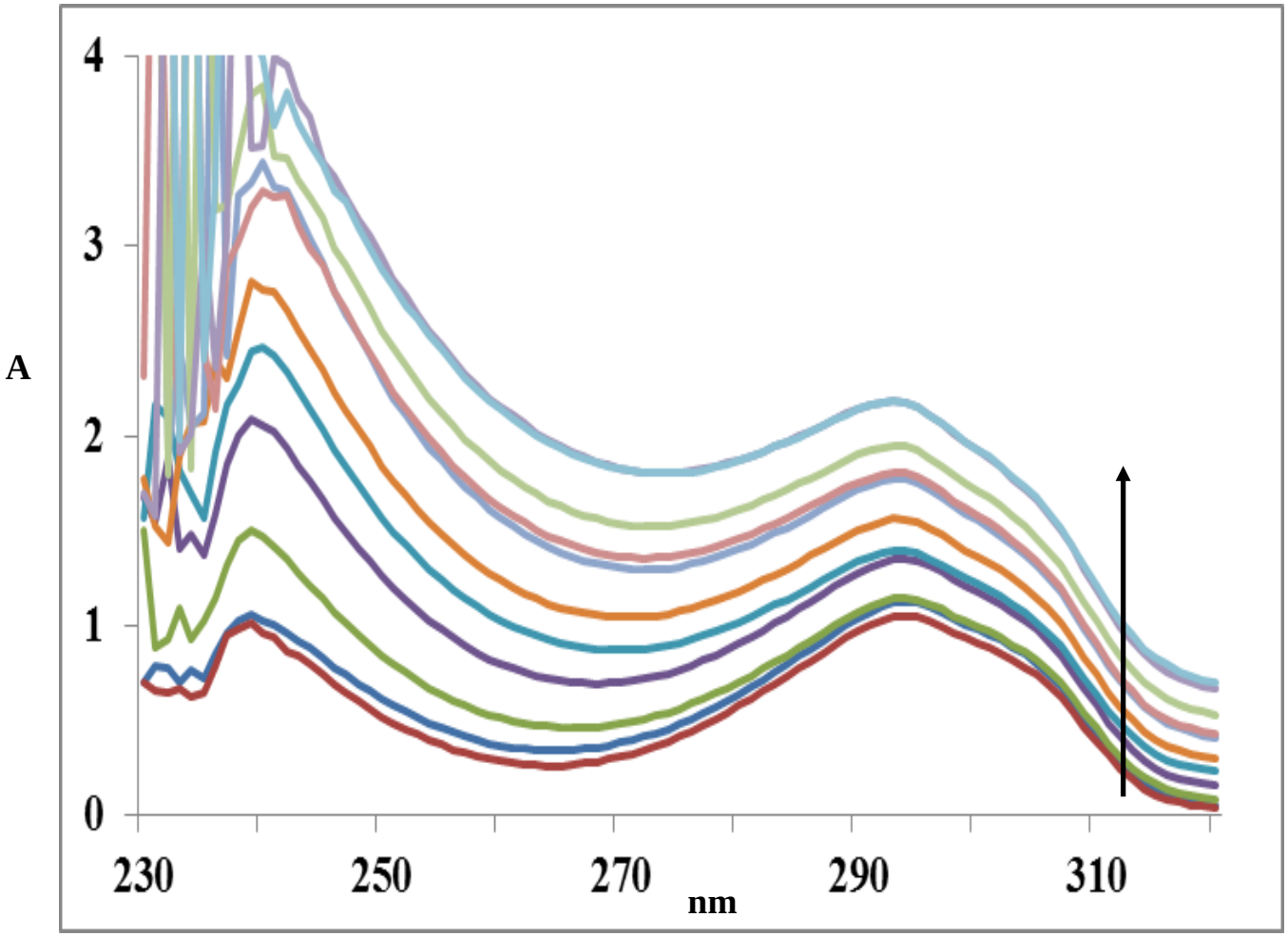

Fig. S18. The spectrophotometric titration of the system pillar[5]arene 5 and $NaNO_3$ in $CHCl_3$ + 5% CH_3OH.

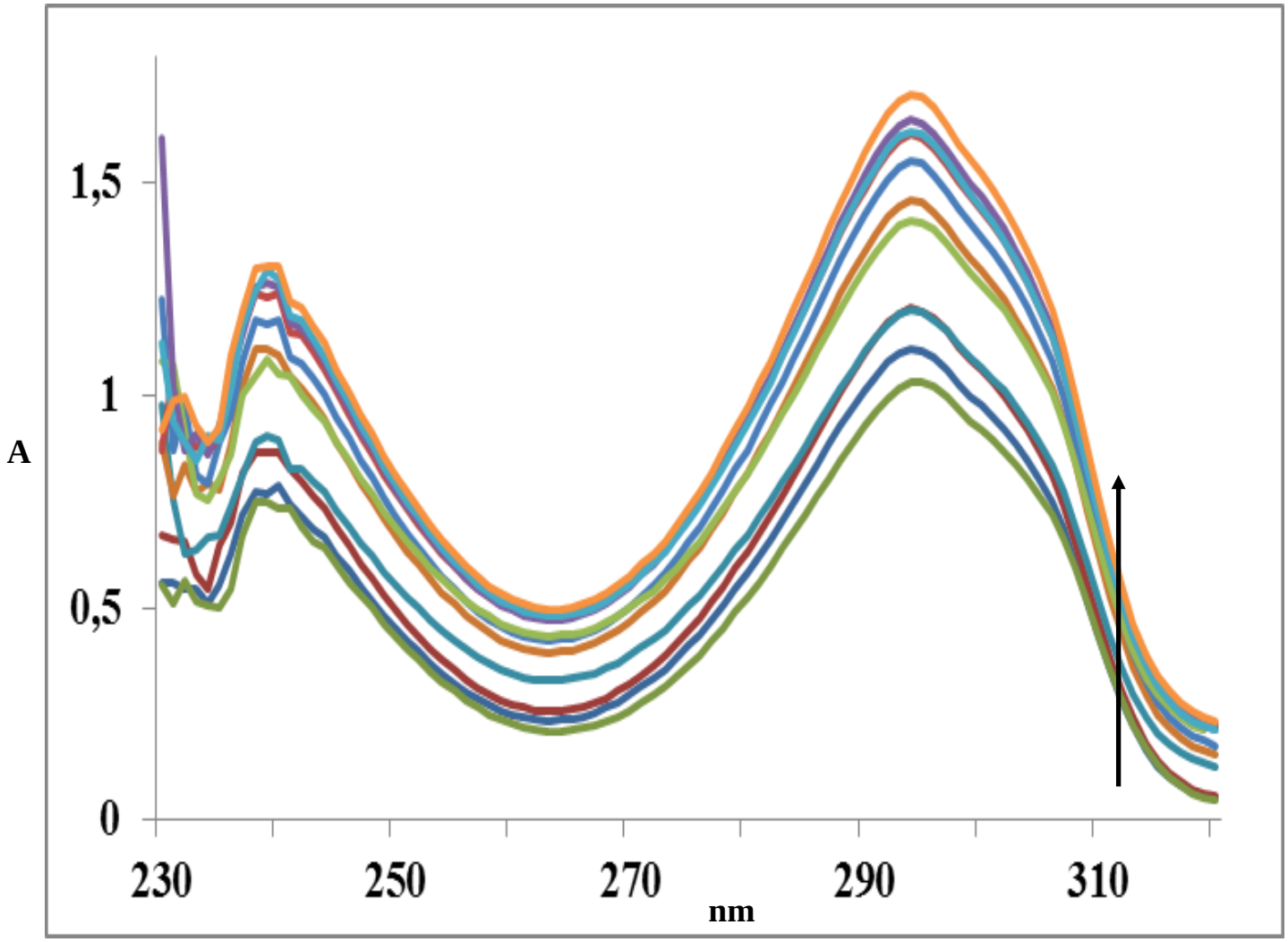

Fig. S19. The spectrophotometric titration of the system pillar[5]arene 5 and $Pb(NO_3)_2$ in $CHCl_3$ + 5% CH_3OH.

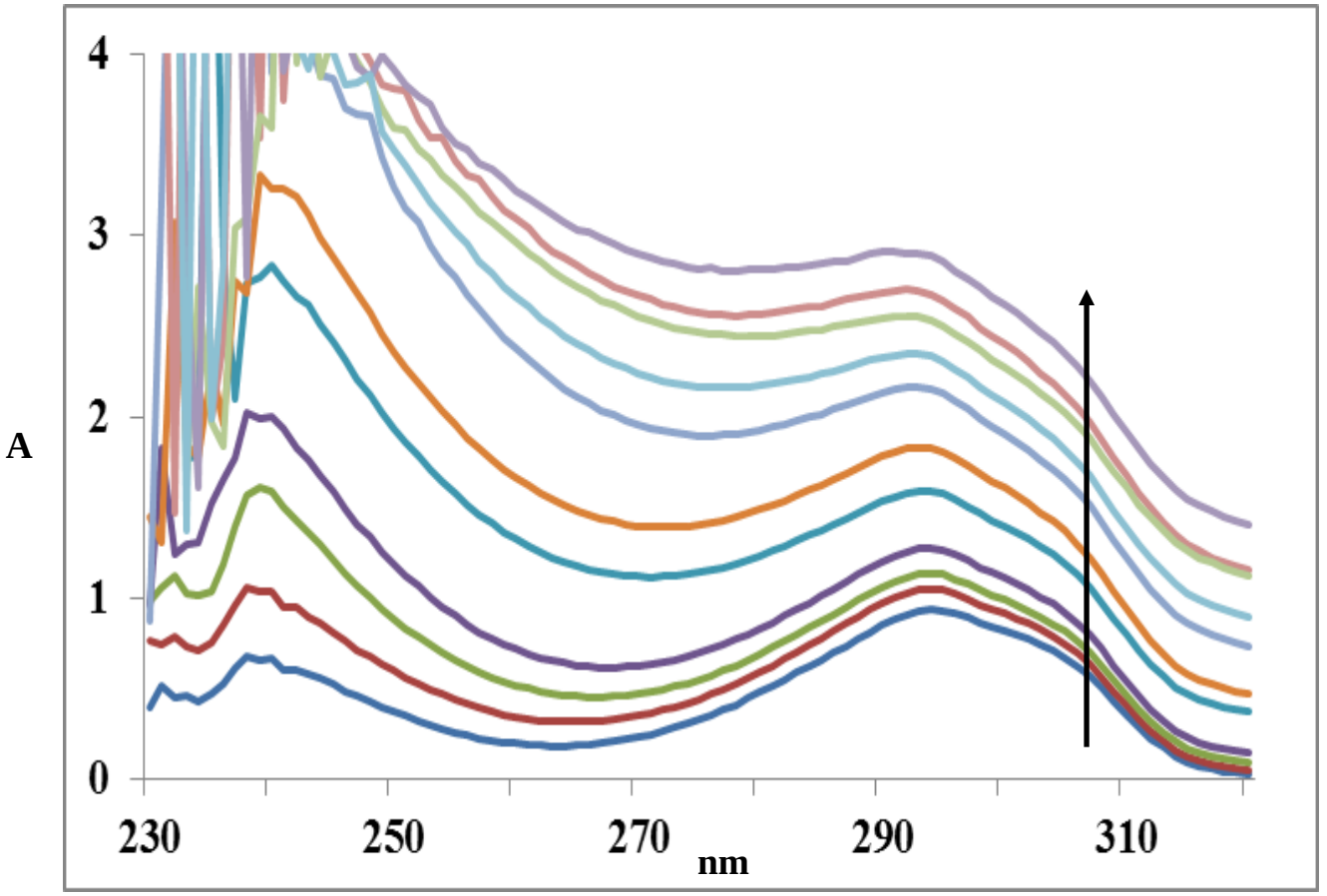

Fig. S20. The spectrophotometric titration of the system pillar[5]arene 6 and KNO_3 in $CHCl_3$ + 5% CH_3OH.

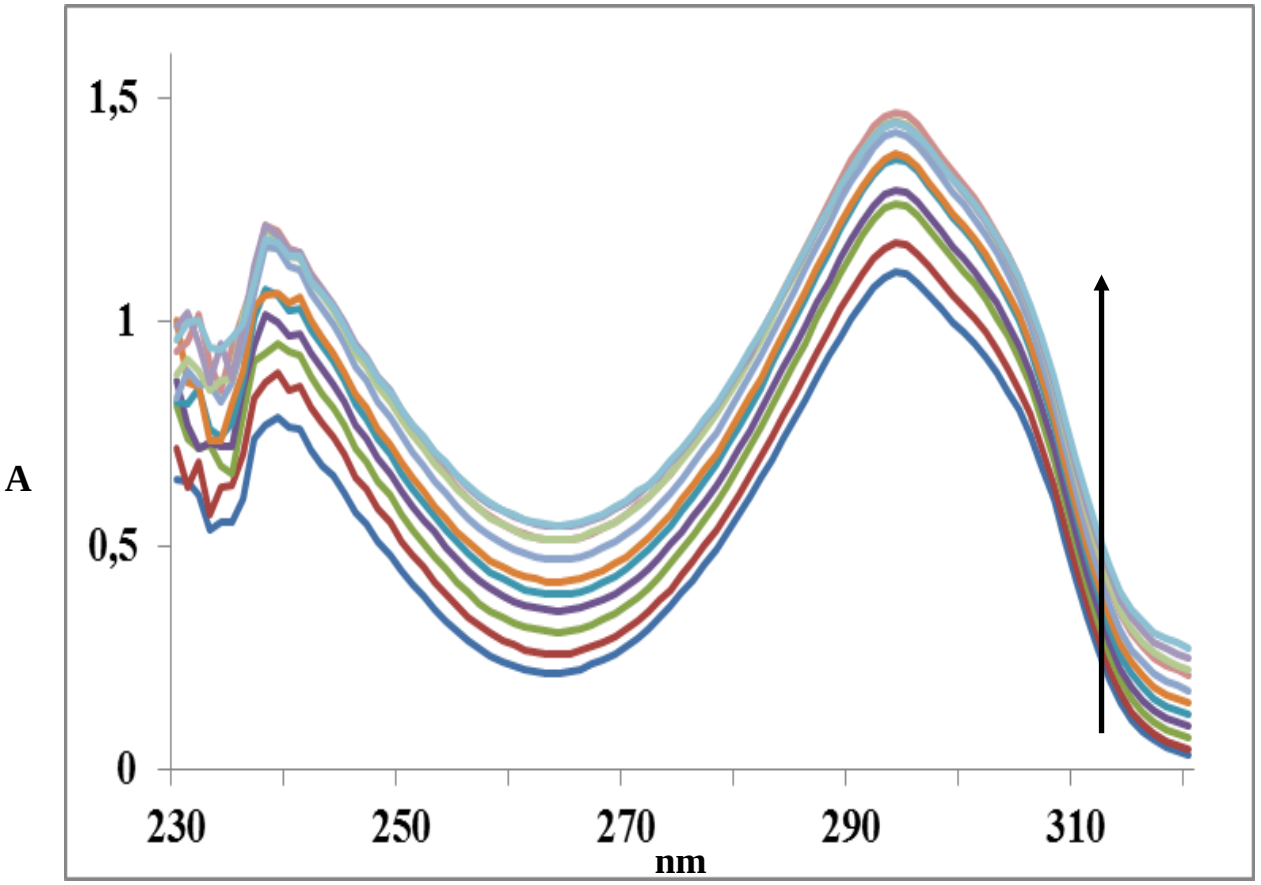

Fig. S21. The spectrophotometric titration of the system pillar[5]arene 6 and $CsNO_3$ in $CHCl_3$ + 5% CH_3OH.

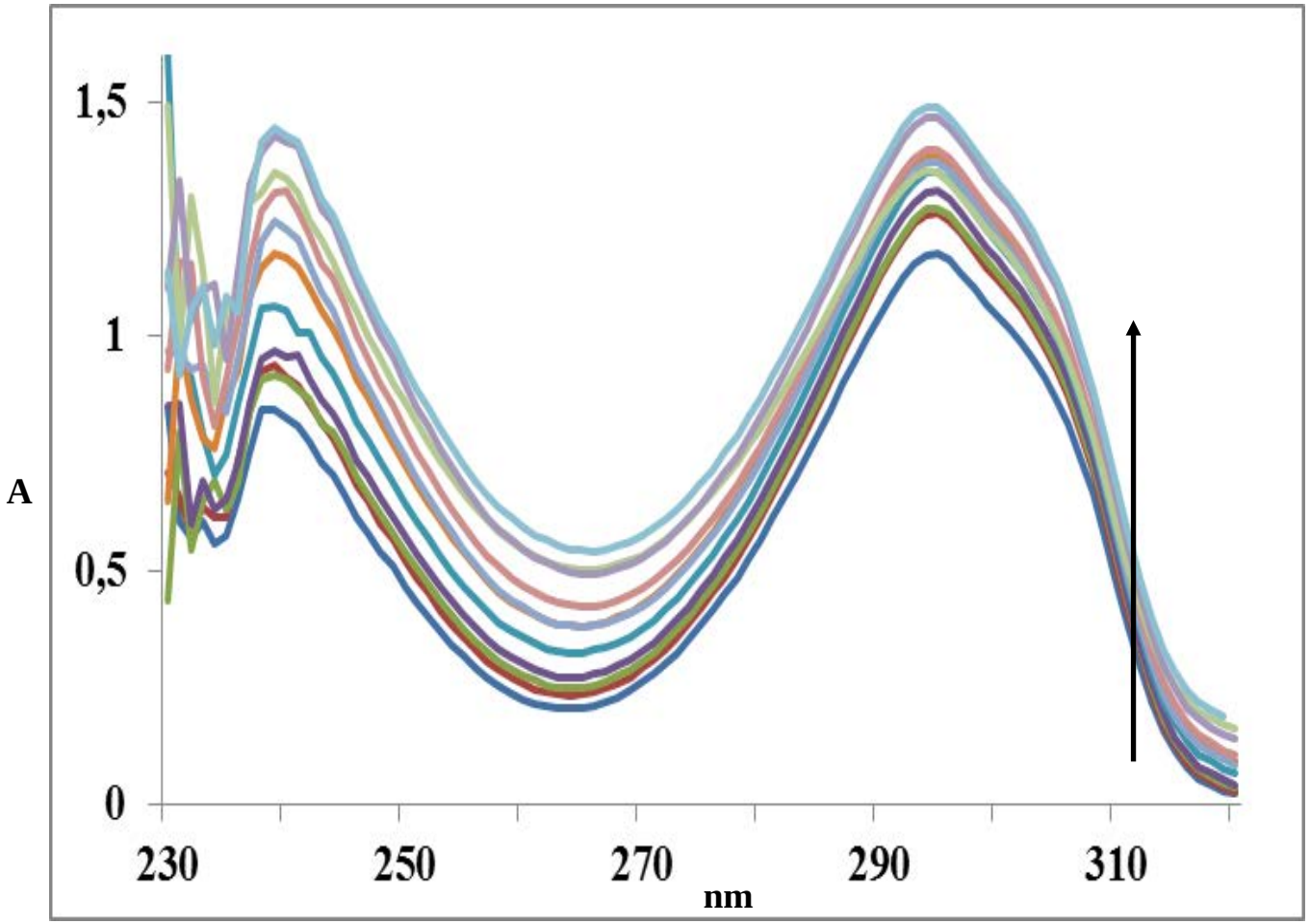

Fig. S22. The spectrophotometric titration of the system pillar[5]arene 6 and $Pb(NO_3)_2$ in $CHCl_3$ + 5% CH_3OH.

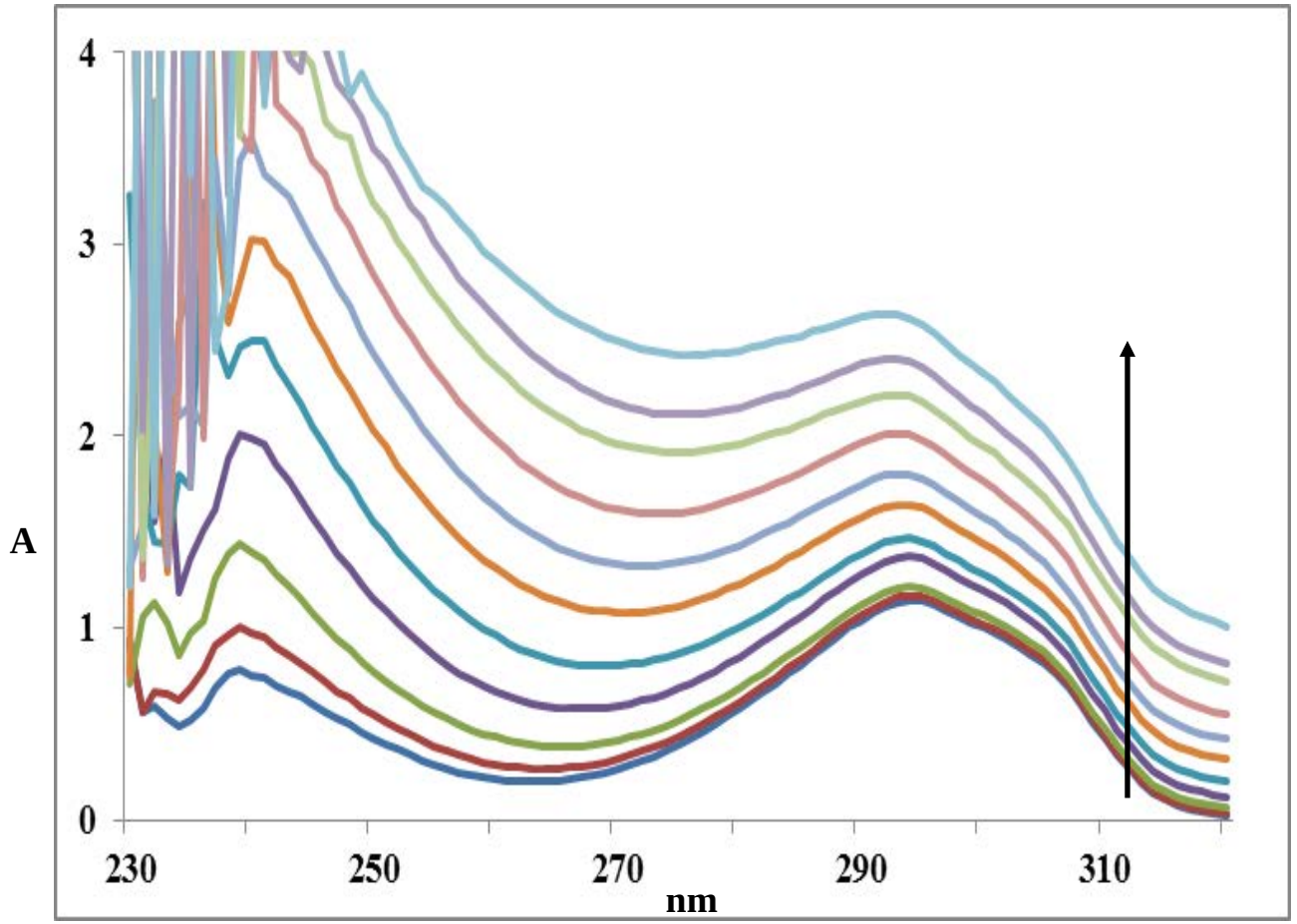

Job Plots

Series of the solutions of pillar[5]arene derivatives **3-6** and metal nitrates ($NaNO_3$, KNO_3, $CsNO_3$, $Pb(NO_3)_2$) were prepared in methanol. The volume of the host and guest solutions varied from 0.6:2.4 to 2.4:0.6, respectively, with the total concentration of the host (H) and guest (G) being constant and equal to $1 \cdot 10^{-5}$ M. The solutions were used without further stirring. The absorbance A_i of the complexation systems was measured at the maximum absorbance wavelength of the complex. The absorbance values were used to plot a diagram from which maximum the structures of the complexes were deduced. Three independent experiments were carried out for each system.

Fig. S23. a) the Job's plot for the determination of the stoichiometry in the complex of the system pillar[5]arene 6 and Pb^{2+} in $CHCl_3$/MeOH; b) the Job's plot for the determination of the stoichiometry in the complex of the system pillar[5]arene 6 and K^+ in $CHCl_3$/MeOH.

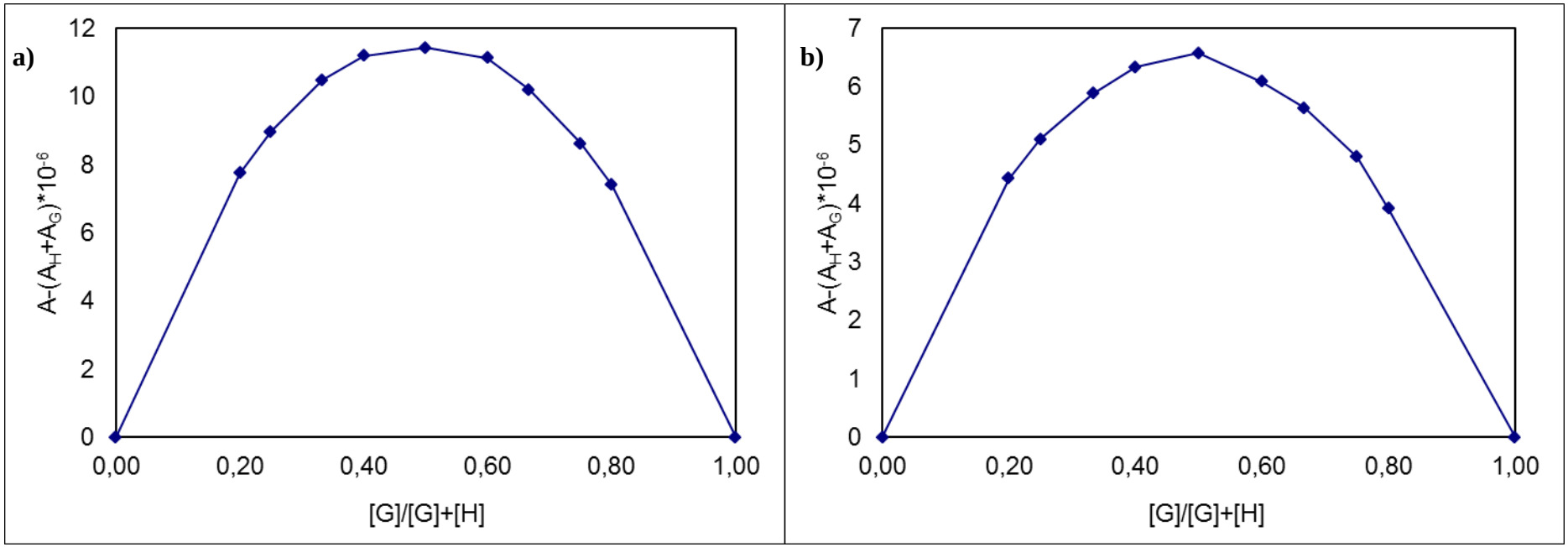

Fig. S24. a) the Job's plot for the determination of the stoichiometry in the complex of the system pillar[5]arene 5 and Pb^{2+} in $CHCl_3$/MeOH; b) the Job's plot for the determination of the stoichiometry in the complex of the system pillar[5]arene 5 and Na^+ in $CHCl_3$/MeOH.

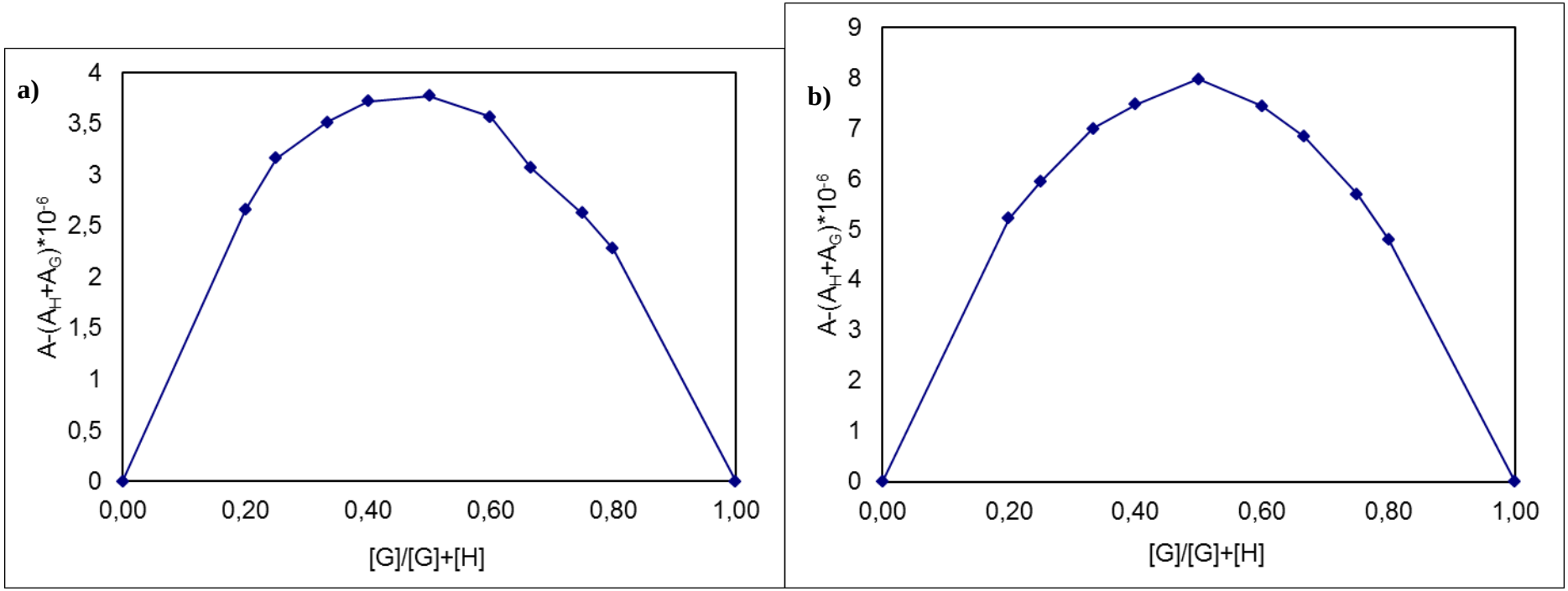

Fig. S25. a) the Job's plot for the determination of the stoichiometry in the complex of the system pillar[5]arene 4 and Cs^+ in $CHCl_3$/MeOH; b) the Job's plot for the determination of the stoichiometry in the complex of the system pillar[5]arene 4 and Na^+ in $CHCl_3$/MeOH.

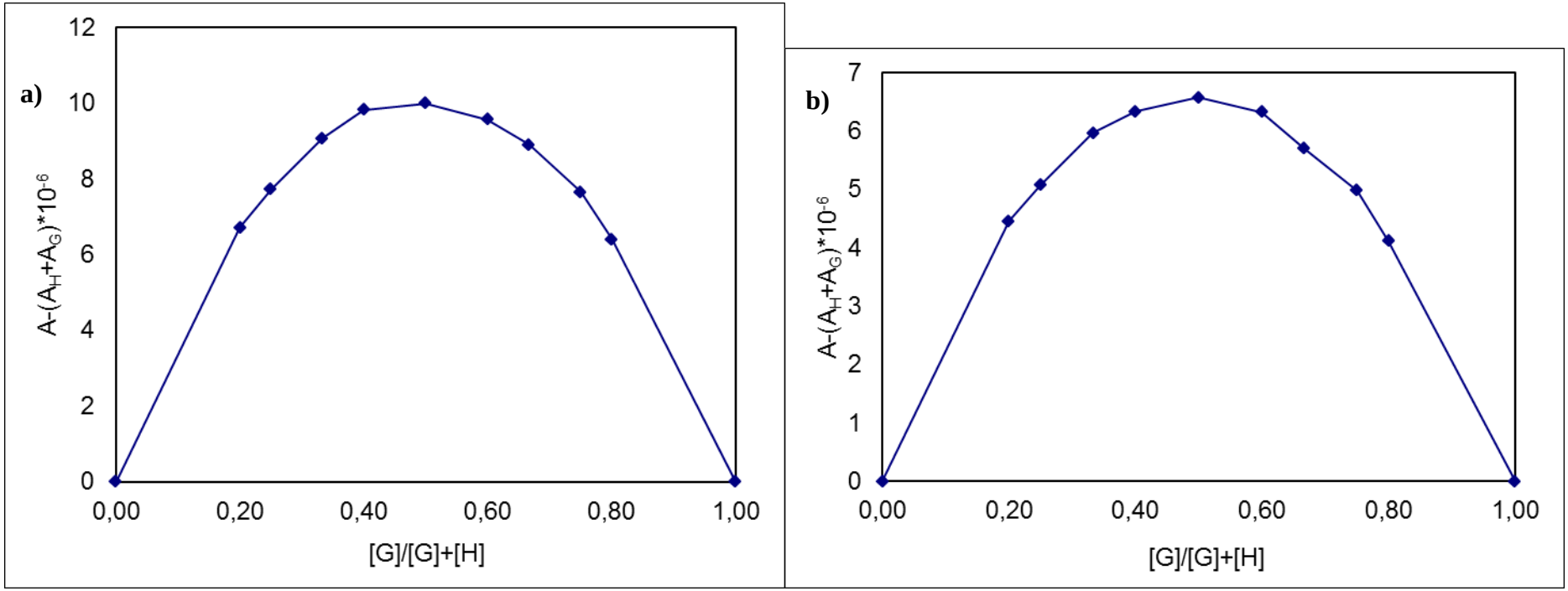

Fig. S26. The Job's plot for the determination of the stoichiometry in the complex of the system pillar[5]arene 3 and Cs^+ in $CHCl_3$/MeOH.

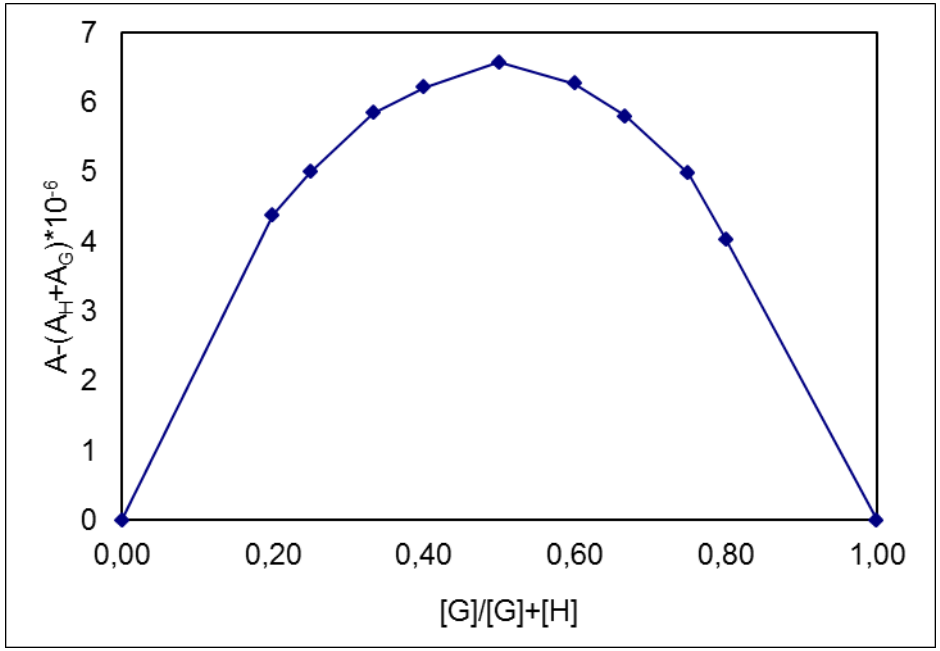

Fig. S27. $^{31}P\{^{1}H\}$ NMR spectra ($CDCl_3$ + 5% CD_3OD, 298 K, 400 MHz): a) 3 (5×10^{-3} M); b) 3 (5×10^{-3} M) + Pb (5×10^{-3} M).

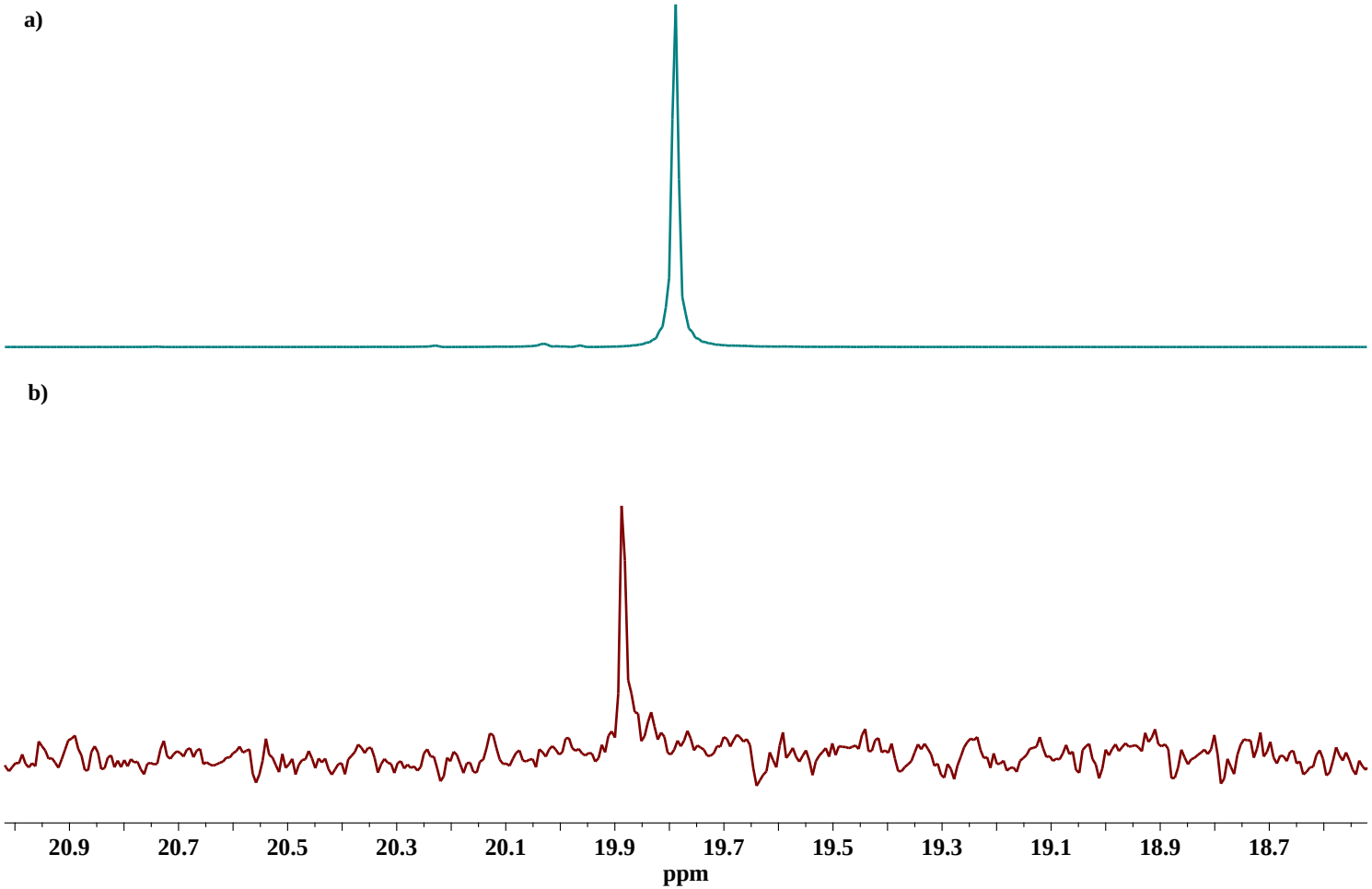

Fig. S28. ^{1}H NMR spectra ($CDCl_3$ + 5% CD_3OD, 298 K, 400 MHz): a) 3 (5×10^{-3} M); b) 3 (5×10^{-3} M) + Pb (5×10^{-3} M).

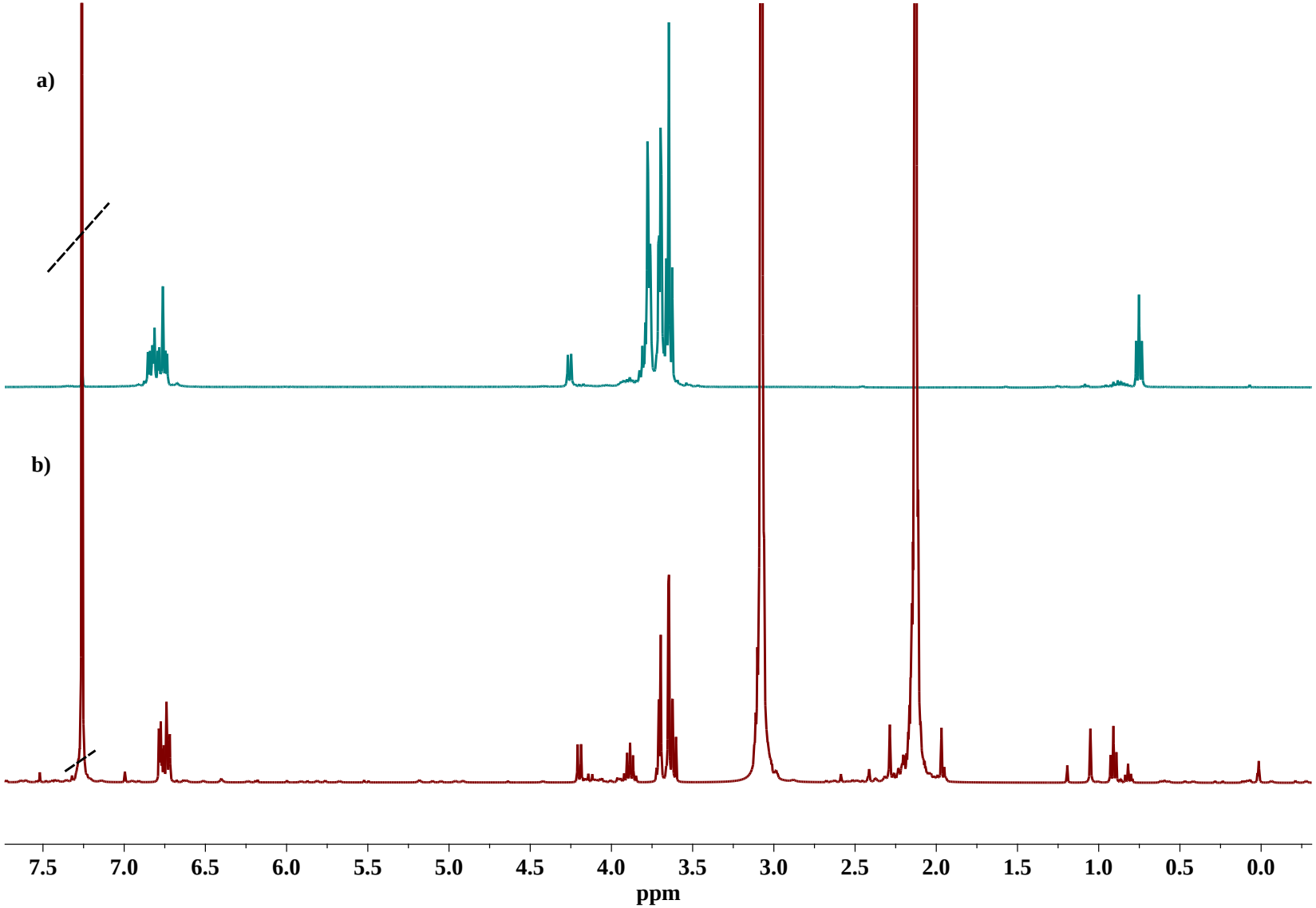

Fig. S29. $^{31}P\{^{1}H\}$ NMR spectra ($CDCl_3$ + 5% CD_3OD, 298 K, 400 MHz): a) 6 (5×10^{-3} M); b) 6 (5×10^{-3} M) + Pb (5×10^{-3} M).

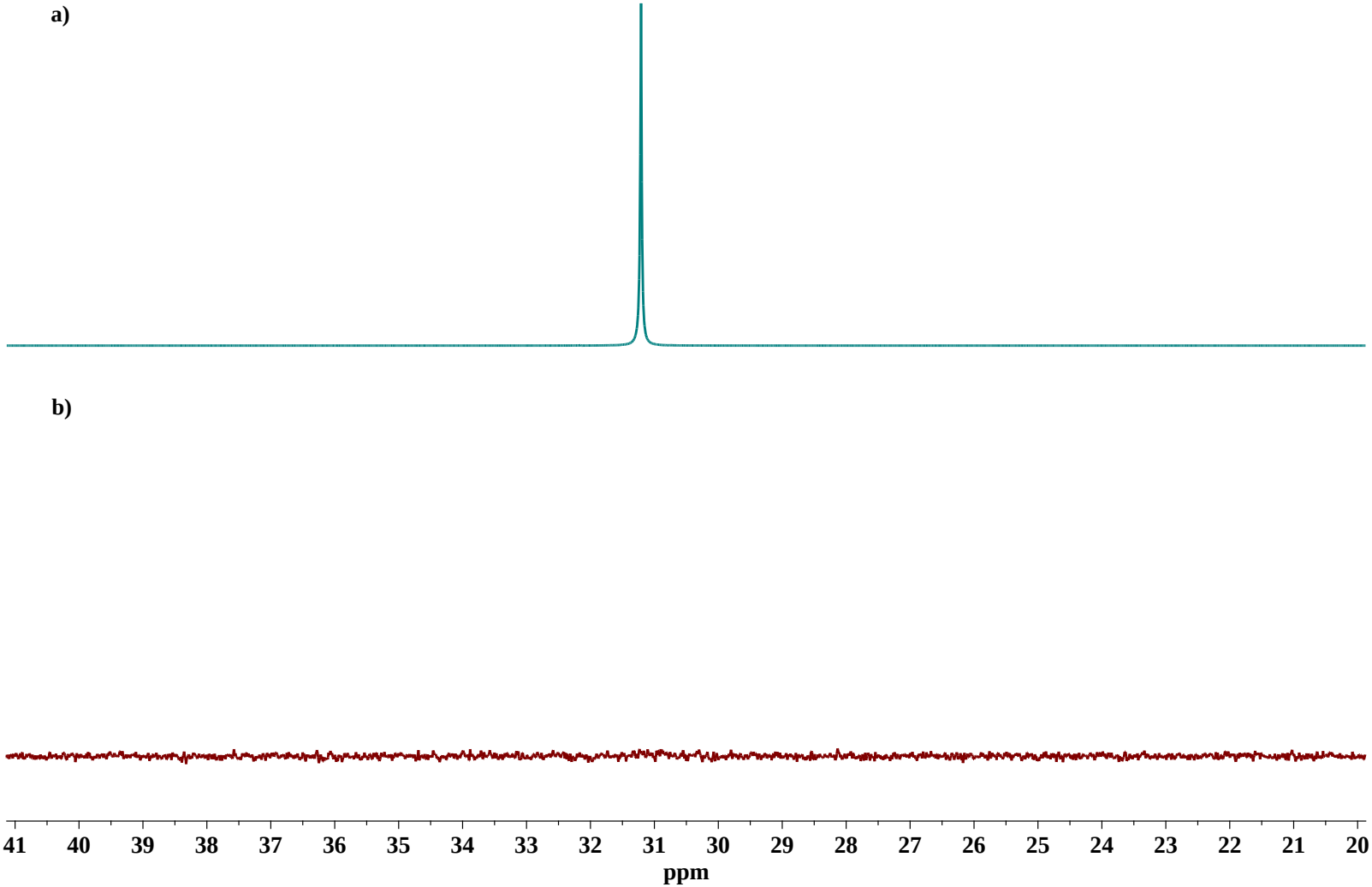

Fig. S30. ^{1}H NMR spectra ($CDCl_3$ + 5% CD_3OD, 298 K, 400 MHz): a) 6 (5×10^{-3} M); b) 6 (5×10^{-3} M) + Pb (5×10^{-3} M).

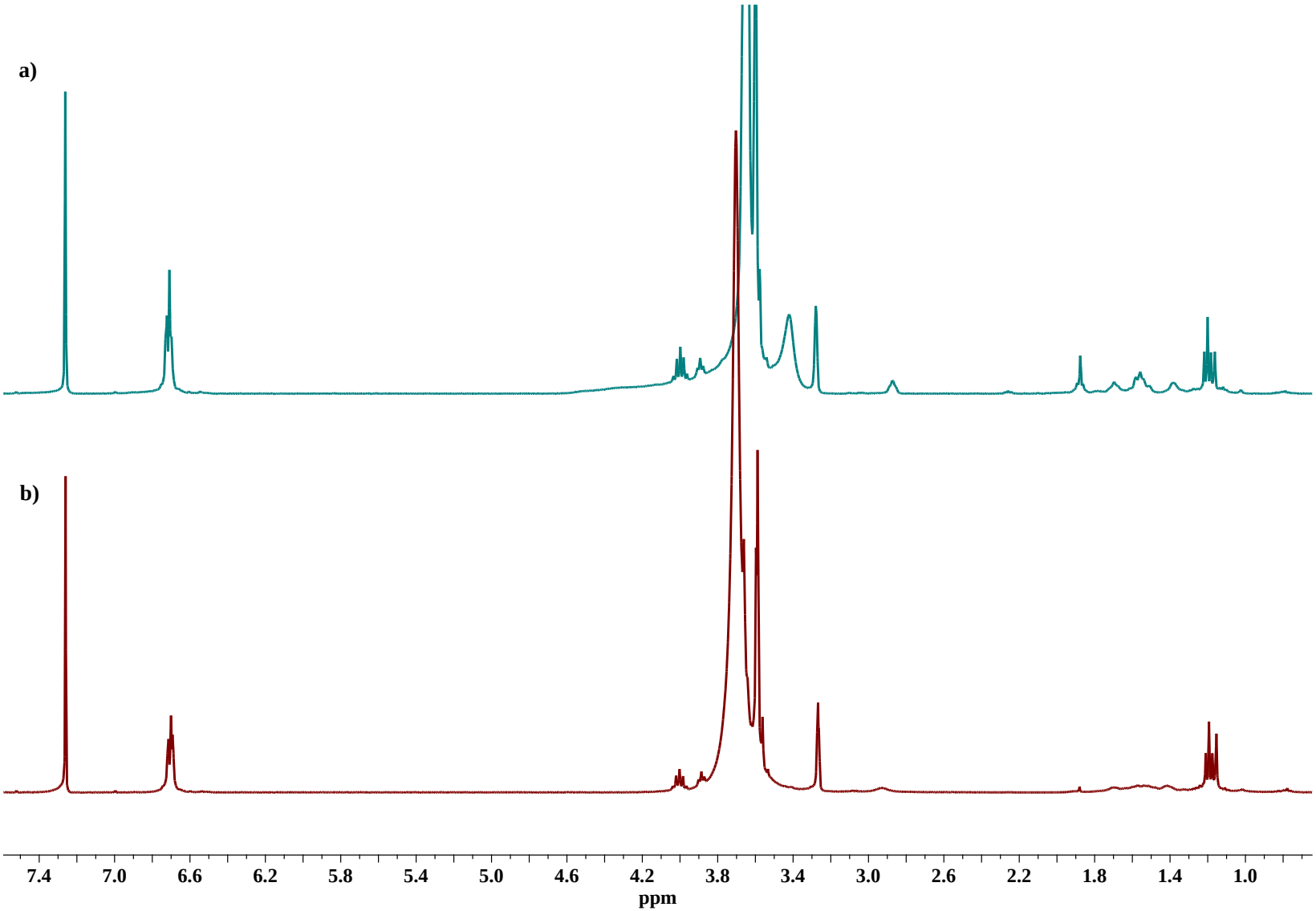

Fig. S31. Size distribution of self-assembles of macrocycle 3 and KNO_3 at C = 1×10^{-4} M in $CHCl_3$.

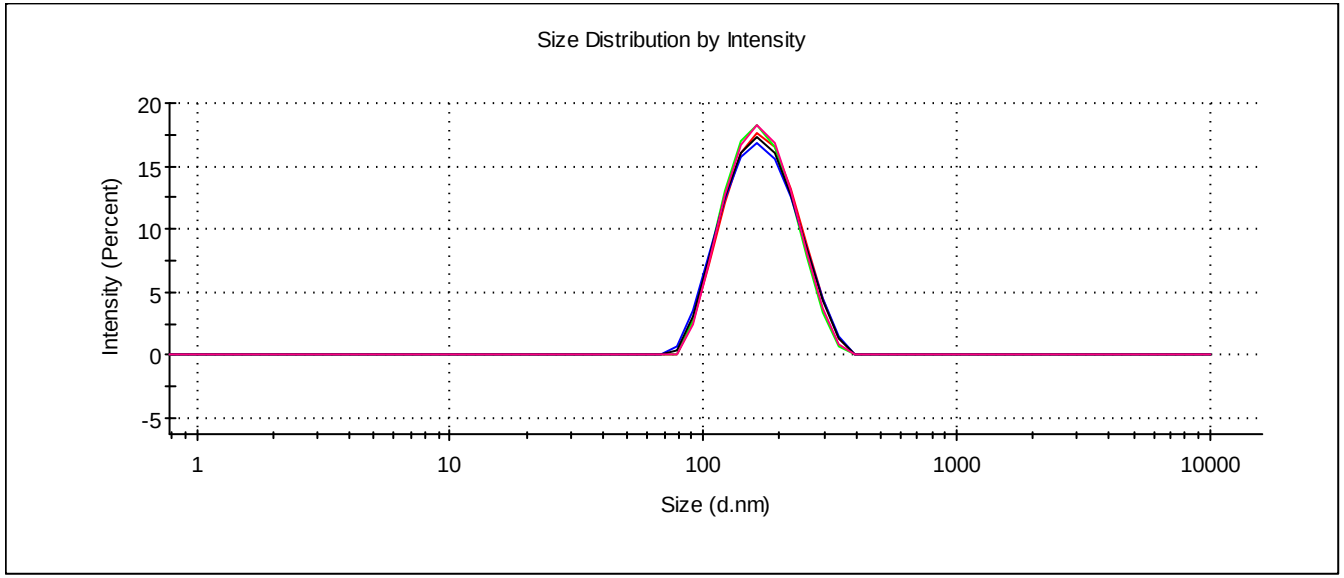

Fig. S32. Size distribution of self-assembles of macrocycle 3 and $CsNO_3$ at C = 1×10^{-3} M in $CHCl_3$.

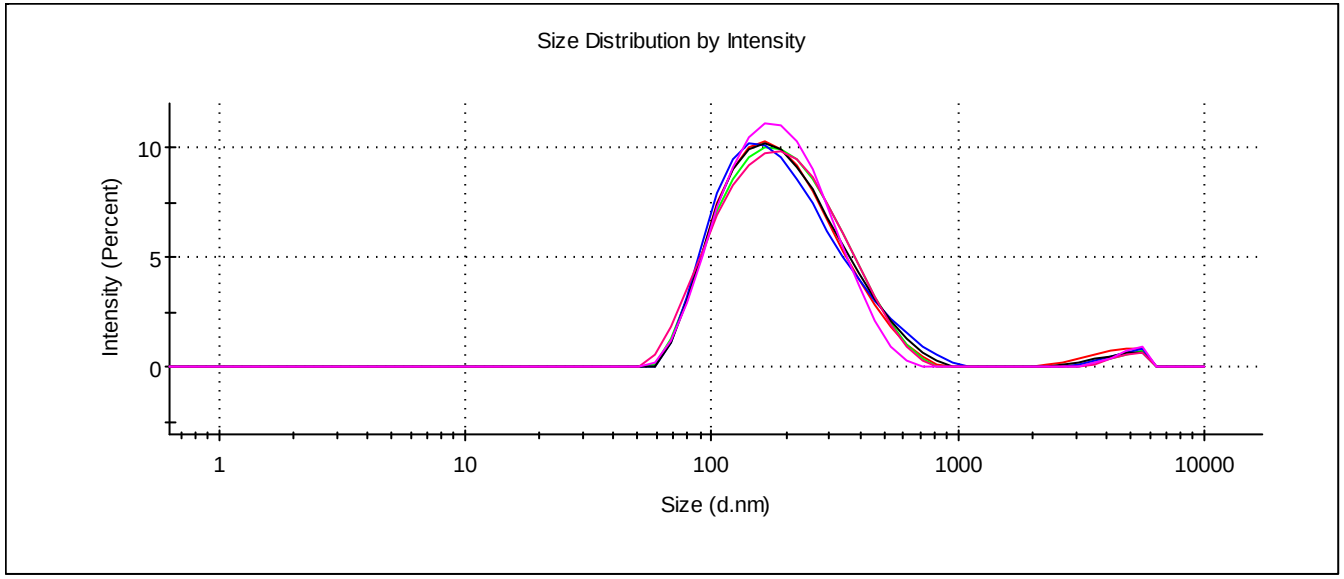

Fig. S33. Size distribution of self-assembles of macrocycle 3 and $Pb(NO_3)_2$ at C = 1×10^{-4} M in $CHCl_3$.

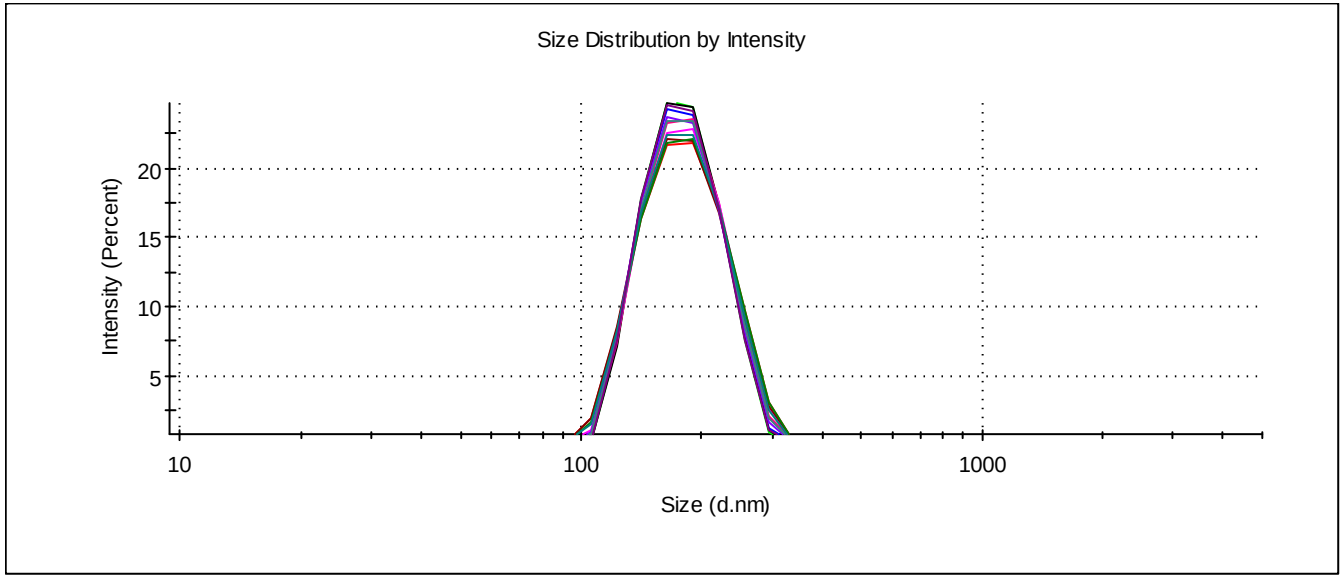

Fig. S34. Size distribution of self-assembles of macrocycle 4 and KNO_3 at C = 1×10^{-3} M in $CHCl_3$.

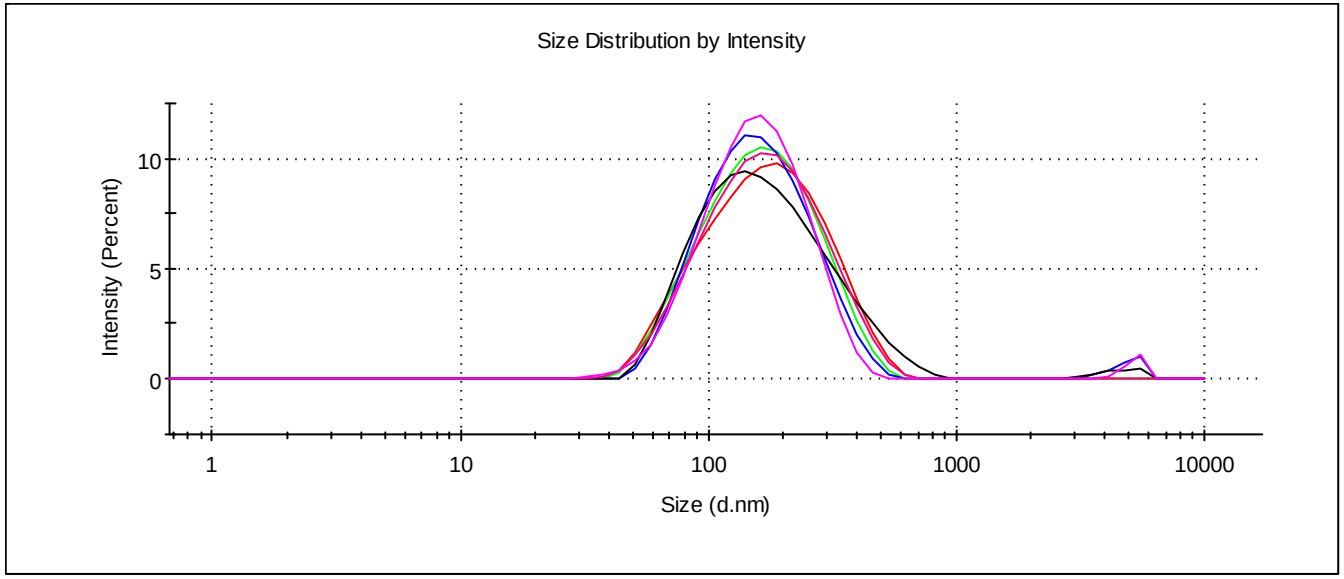

Fig. S35. Size distribution of self-assembles of macrocycle 4 and $CsNO_3$ at C = 1×10^{-3} M in $CHCl_3$.

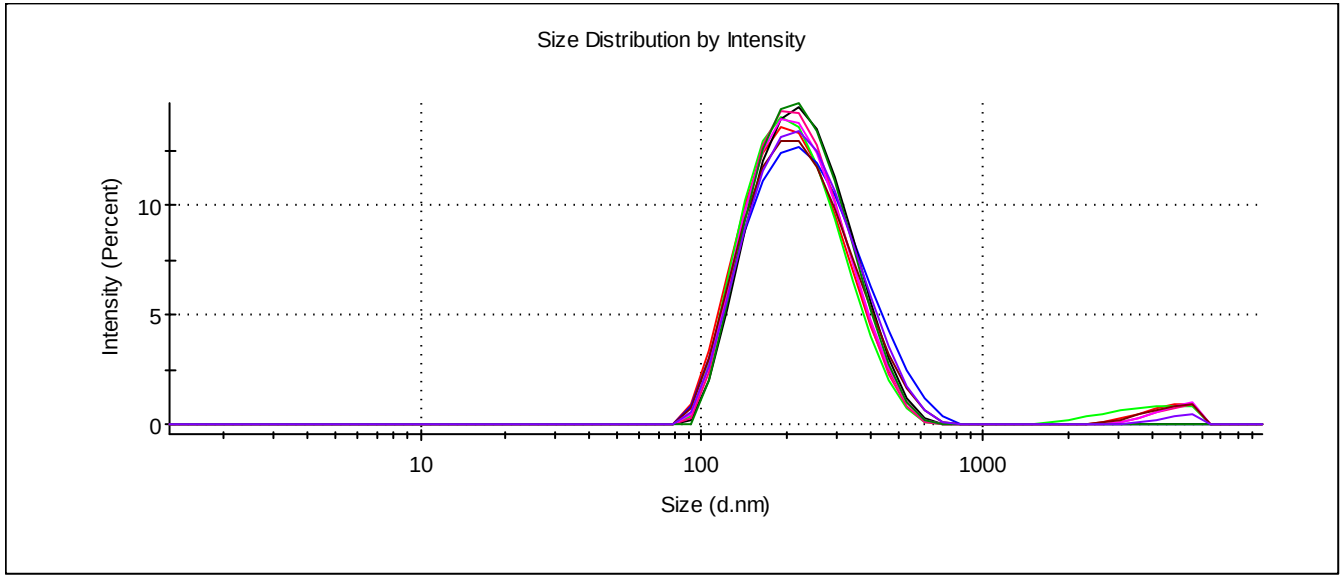

Fig. S36. Size distribution of self-assembles of macrocycle 4 and $Pb(NO_3)_2$ at C = 1×10^{-4} M in $CHCl_3$.

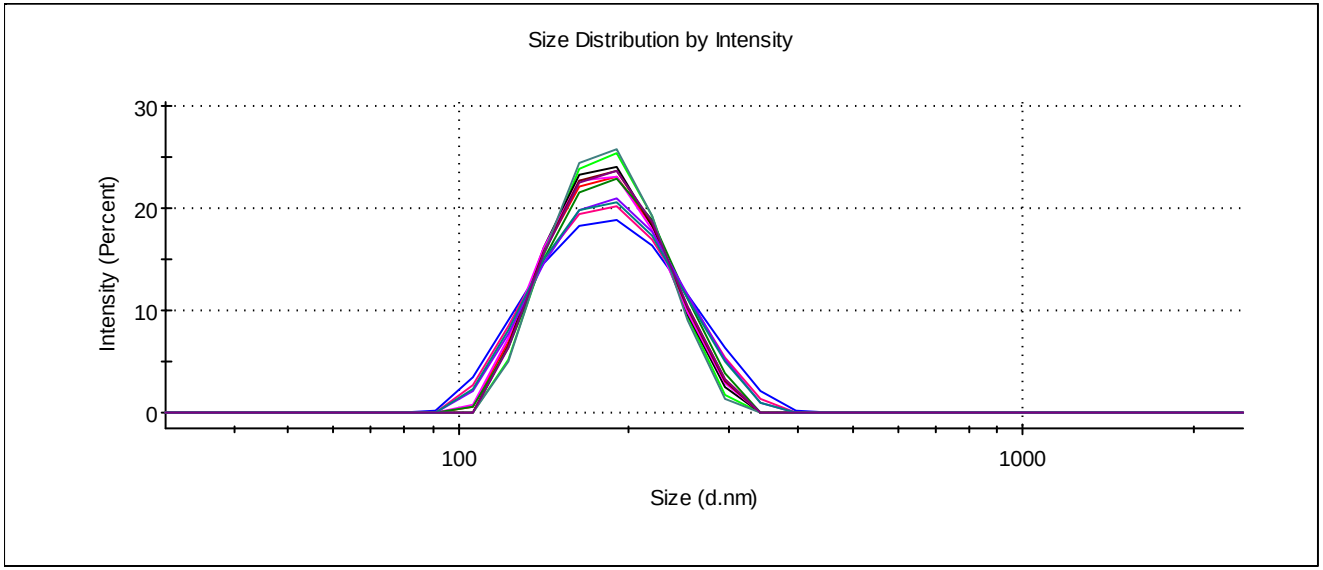

Fig. S37. Size distribution of self-assembles of macrocycle 5 and KNO_3 at C = 1×10^{-4} M in $CHCl_3$.

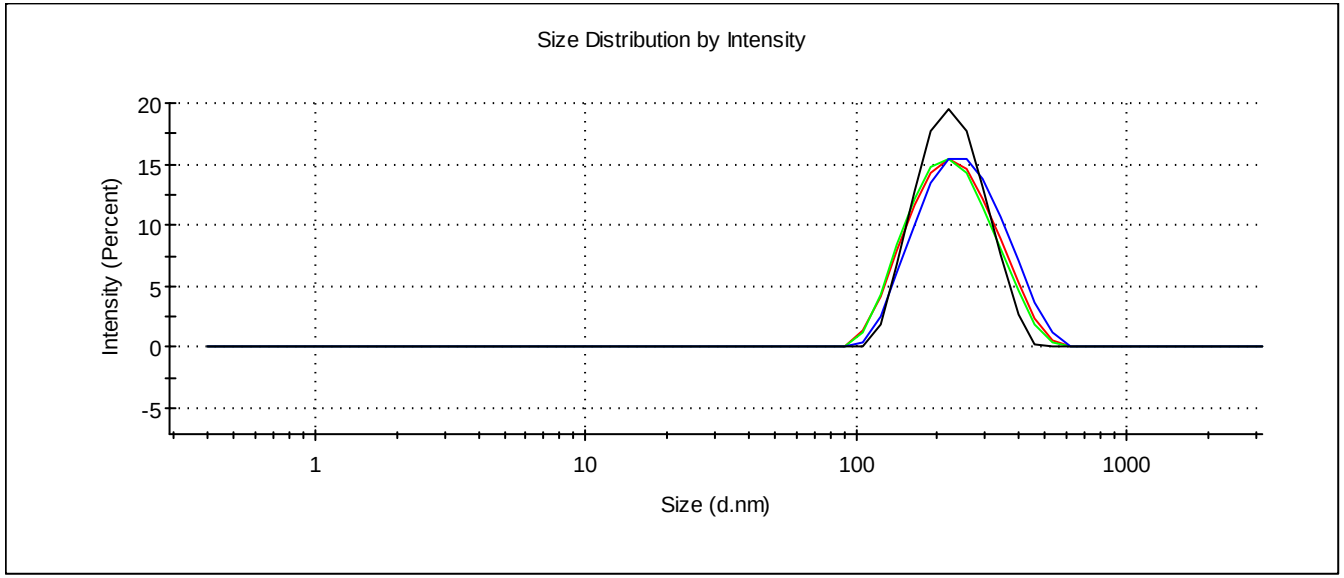

Fig. S38. Size distribution of self-assembles of macrocycle 5 and $CsNO_3$ at C = 1×10^{-4} M in $CHCl_3$.

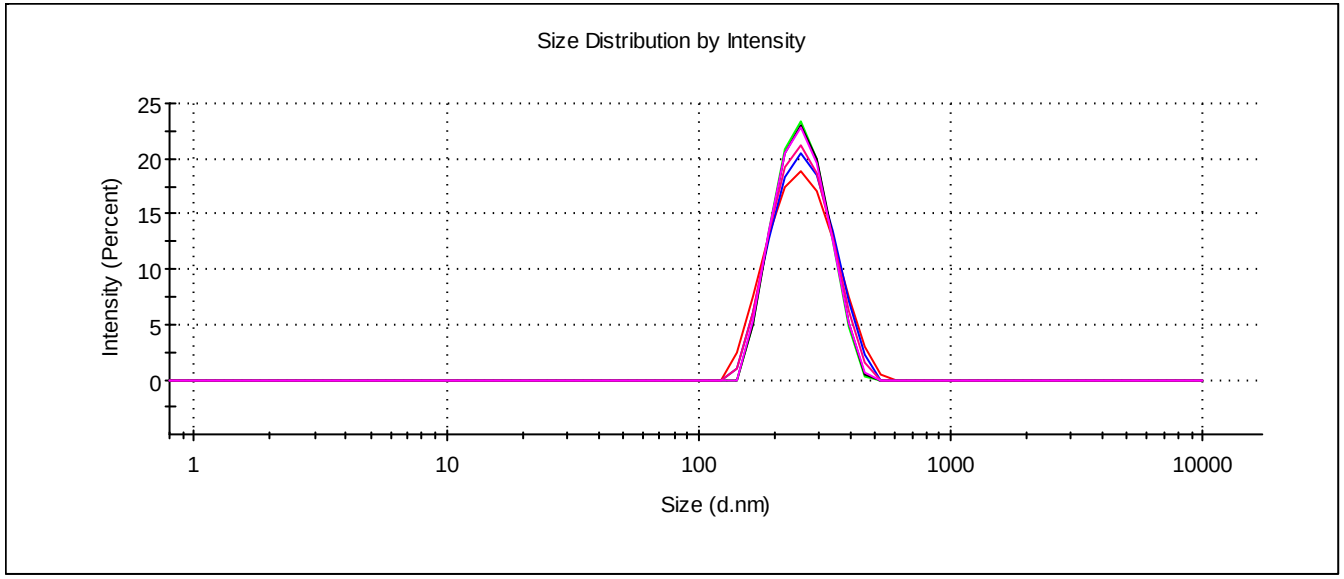

Fig. S39. Size distribution of self-assembles of macrocycle 5 and $Pb(NO_3)_2$ at C = 1×10^{-5} M in $CHCl_3$.

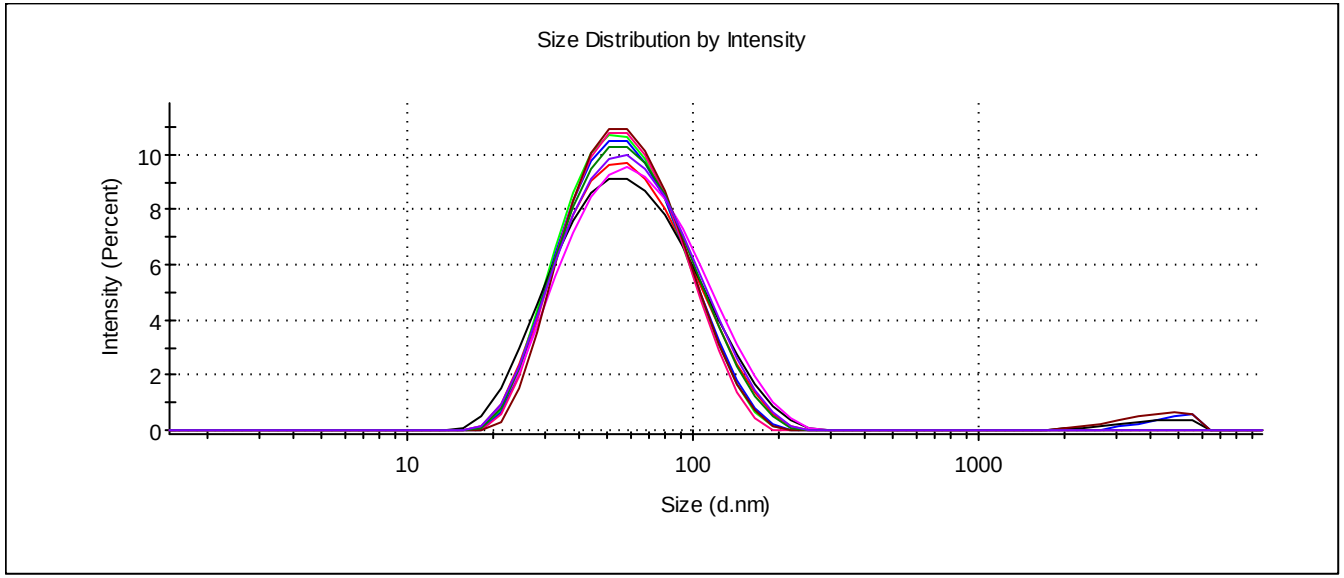

Fig. S40. Size distribution of self-assembles of macrocycle 6 and KNO_3 at C = 1×10^{-3} M in $CHCl_3$.

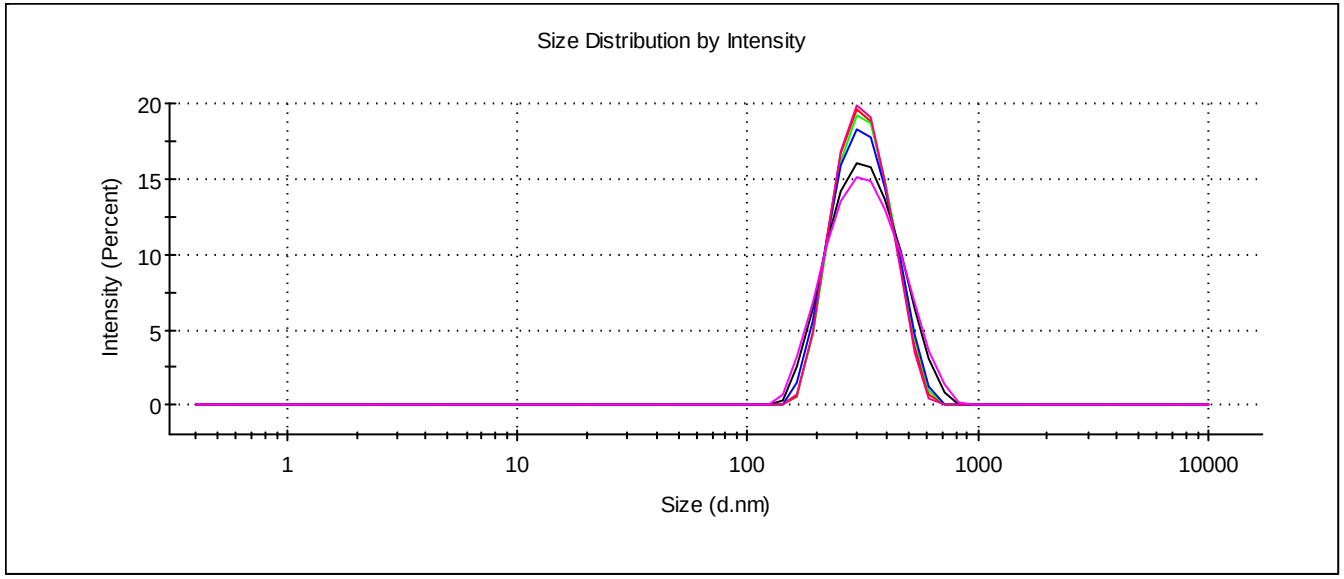

Fig. S41. Size distribution of self-assembles of macrocycle 6 and $CsNO_3$ at C = 1×10^{-4} M in $CHCl_3$.

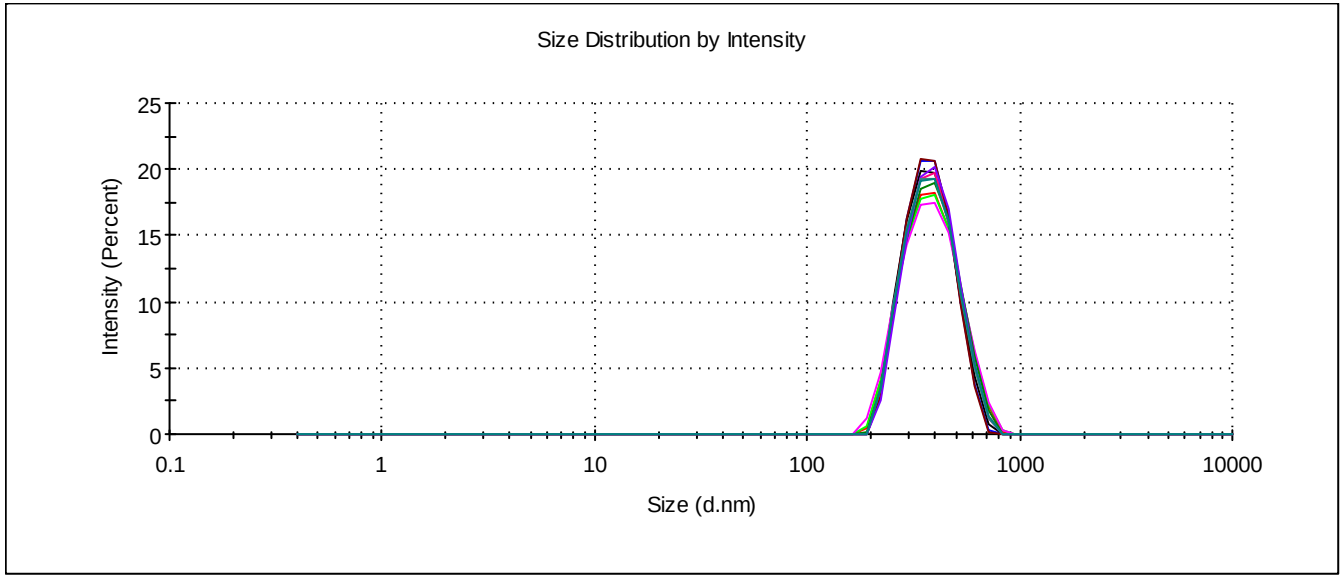

Fig. S42. Size distribution of self-assembles of macrocycle 6 and $Pb(NO_3)_2$ at C = 1×10^{-4} M in $CHCl_3$.

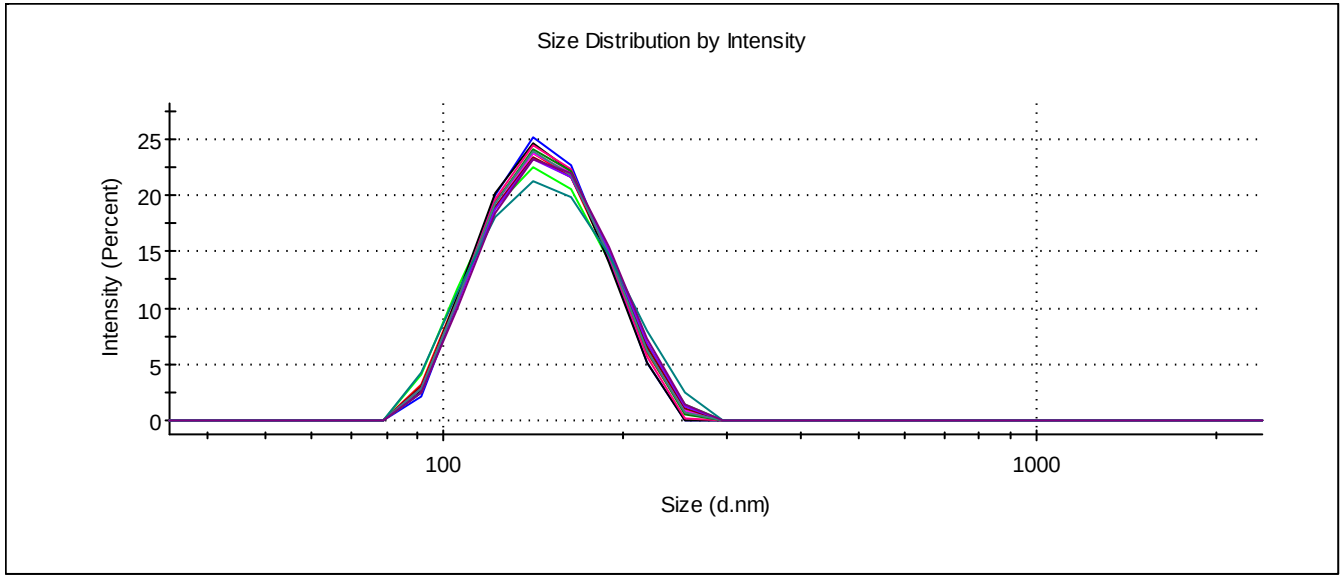

Fig. S43. Energy-dispersion spectrum of fractal structure formed by pillar[5]arene **3** and Pb^{2+} on the copper support. On the insert a) supramolecular nanometer-sized aggregates formed by the compound **3** and Pb^{2+}; b) mapping of P; c) superposition of elemental maps of P and Pb in the spherical aggregates formed by pillar[5]arene **3** and Pb^{2+}; d) mapping of Pb^{2+}**.**

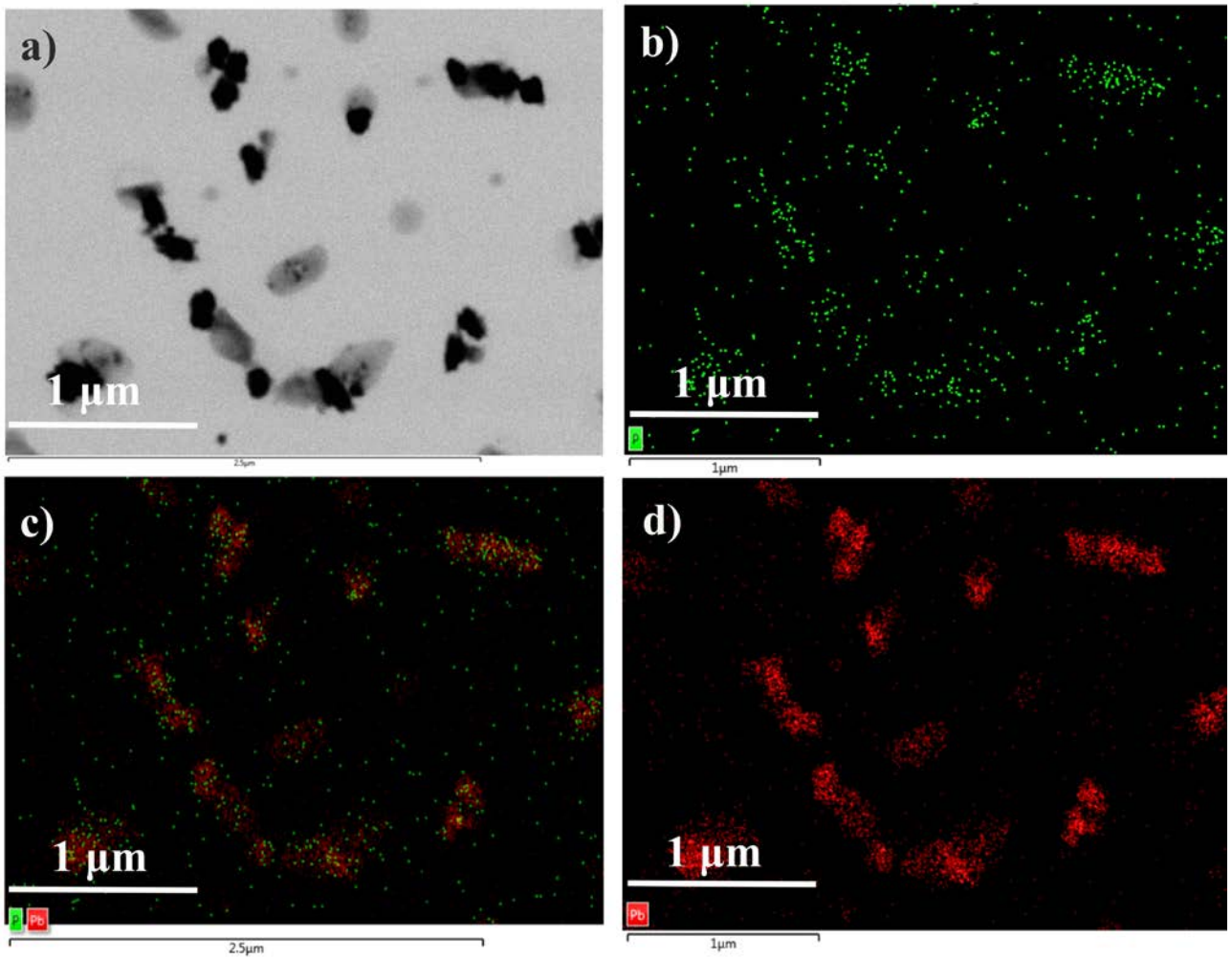

Fig. S44. Energy-dispersion spectrum of fractal structure formed by pillar[5]arene **4** and Pb^{2+} on the copper support. On the insert a) supramolecular nanometer-sized aggregates formed by the compound **4** and Pb^{2+}; b) mapping of P; c) superposition of elemental maps of P and Pb in the spherical aggregates formed by pillar[5]arene **4** and Pb^{2+}; d) mapping of Pb^{2+}.

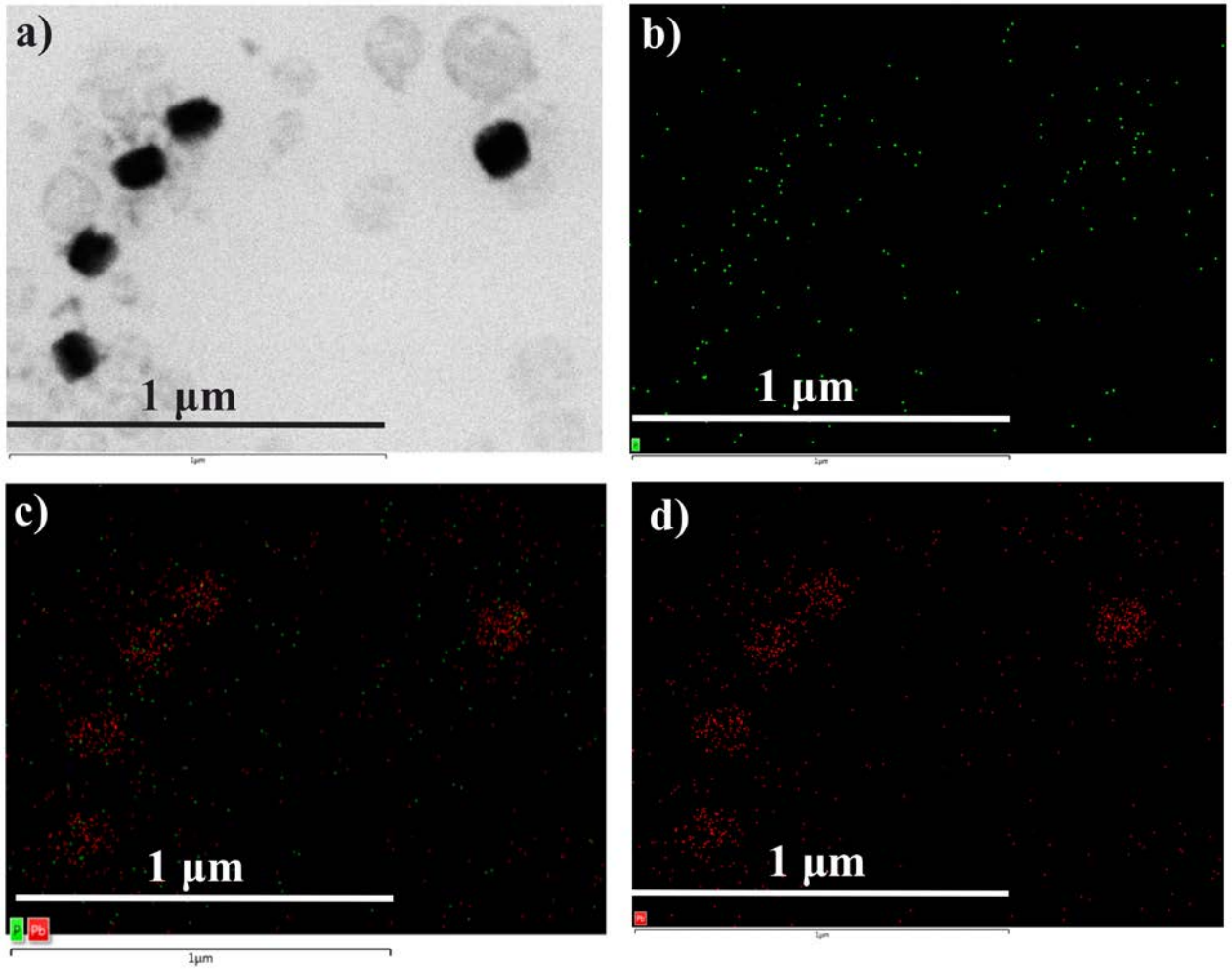

Fig. S45. Energy-dispersion spectrum of fractal structure formed by pillar[5]arene **5** and Pb^{2+} on the copper support. On the insert a) supramolecular nanometer-sized aggregates formed by the compound **5** and Pb^{2+}; b) mapping of P; c) superposition of elemental maps of P and Pb in the spherical aggregates formed by pillar[5]arene **5** and Pb^{2+}; d) mapping of Pb^{2+}.

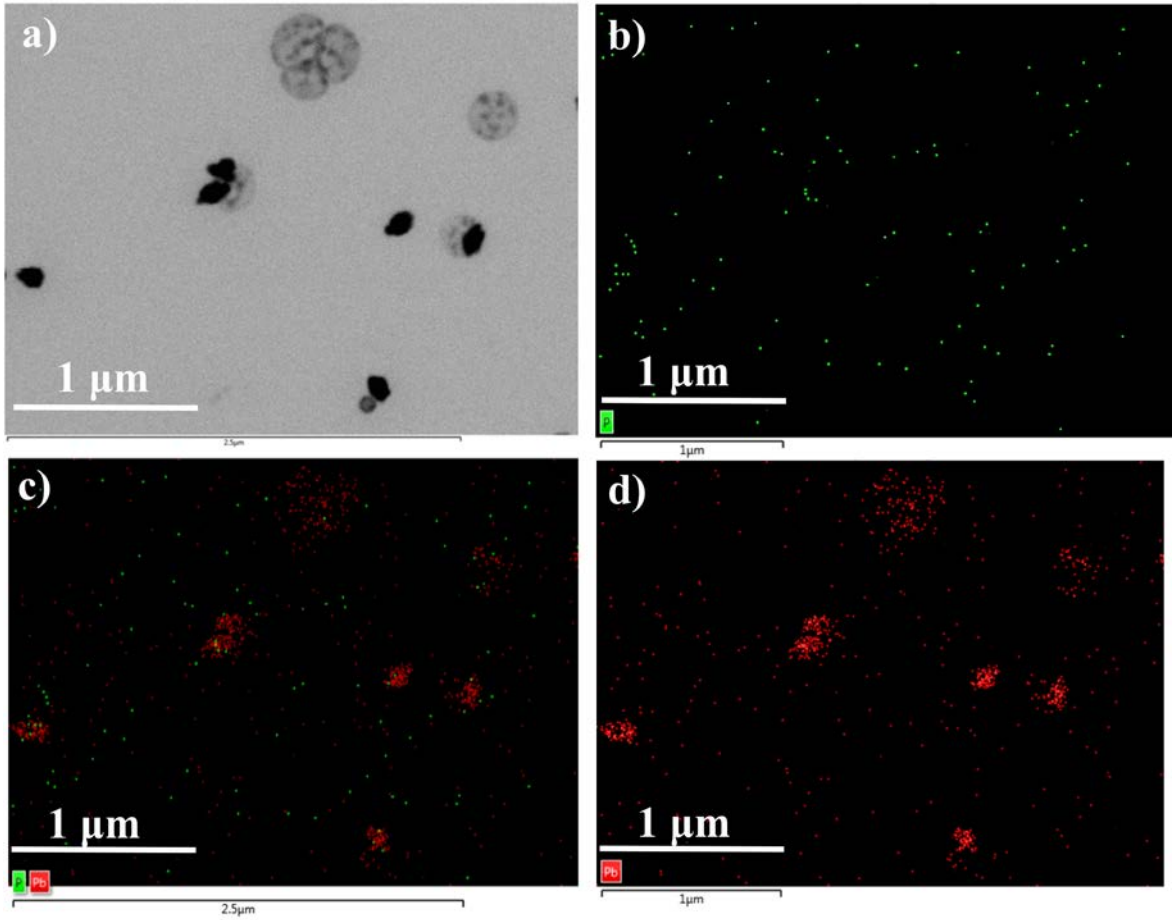

Fig. S46. Energy-dispersion spectrum of fractal structure formed by pillar[5]arene **6** and Pb^{2+} on the copper support. On the insert a) supramolecular nanometer-sized aggregates formed by the compound **6** and Pb^{2+}; b) mapping of P; c) superposition of elemental maps of P and Pb in the spherical aggregates formed by pillar[5]arene **6** and Pb^{2+}; d) mapping of Pb^{2+}.

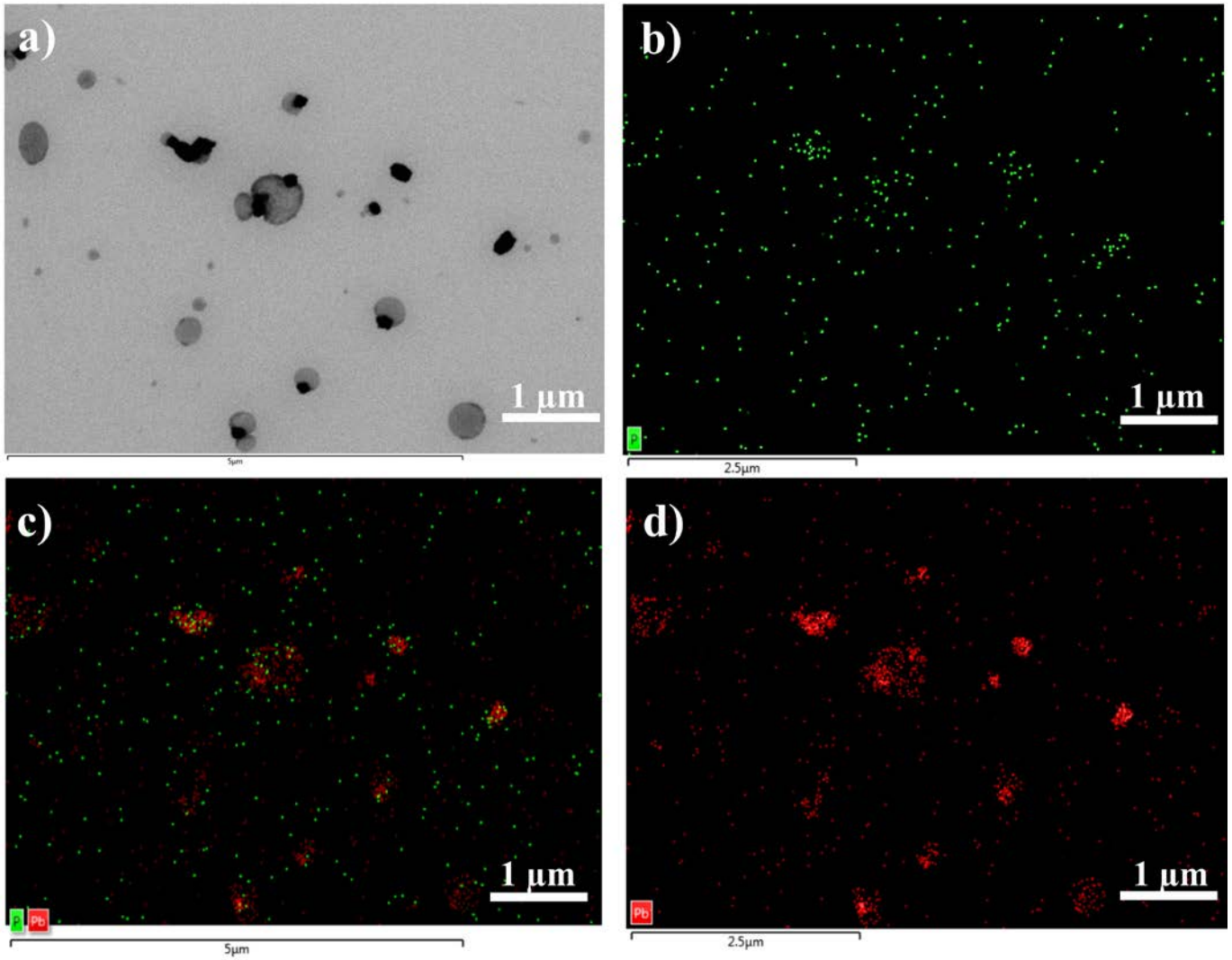

Fig. S47. Endo (left) and exo (right) conformations for pillar[5]arenes **3** (top) to **6** (bottom), hydrogen atoms removed for clarity.